David Sanz Morales

Maximum Power Point Tracking Algorithms for Photovoltaic Applications

Faculty of Electronics, Communications and Automation

Thesis submitted for examination for the degree of Master of Science in Technology.

Espoo 14.12.2010

Thesis supervisor:

Prof. Seppo Ovaska

Thesis instructor:

D.Sc. (Tech.) Konstantin Kostov

A! **Aalto University**
School of Science
and Technology

Author: David Sanz Morales

Title: Maximum Power Point Tracking Algorithms for Photovoltaic Applications

Date: 14.12.2010   Language: English   Number of pages:9+73

Faculty of Electronics, Communications and Automation

Department of Electrical Engineering

Professorship: Power Electronics   Code: S-81

Supervisor: Prof. Seppo Ovaska

Instructor: D.Sc. (Tech.) Konstantin Kostov

Solar panels have a nonlinear voltage-current characteristic, with a distinct *maximum power point* (MPP), which depends on the environmental factors, such as temperature and irradiation. In order to continuously harvest maximum power from the solar panels, they have to operate at their MPP despite the inevitable changes in the environment. This is why the controllers of all solar power electronic converters employ some method for *maximum power point tracking* (MPPT). Over the past decades many MPPT techniques have been published. The first objective of this thesis is to study and analyze them. The three algorithms that where found most suitable for large and medium size *photovoltaic* (PV) applications are *perturb and observe* (P&O), *incremental conductance* (InCond) and *fuzzy logic control* (FLC). These were compared and tested dynamically according a recently issued standard. Several modifications to the P&O and the InCond algorithms are proposed, which overcome their poor performance when the irradiation changes continuously.

The dynamic MPPT efficiency tests require long simulations and if detailed models of the power converter are used they can take a lot of memory and computation time. To overcome this challenge a simplified model of the PV system was developed. This model was validated with simulations.

Keywords: PV power generation, MPPT algorithms, perturb and observe, incremental conductance, fuzzy logic

Tekijä: David Sanz Morales

Työn nimi: Maksimitehopisteen seuraajat aurinkoenergian tuotannossa

Aurinkopaneelien tuottana teho muuttuu epälineaarisesti virran funktiona siten, että on olemassa selkeä toimintapiste, jossa teho on suurimmillaan. Tätä pistettä kutsutaan maksimitehopisteeksi ja se riippuu ulkoisista olosuhteista, kuten lämpötila ja säteilyn voimakkuus. Jotta aurinkopaneeleista saataisiin jatkuvasti suurin mahdollinen teho, täytyy paneeli pitää maksimitehopisteessä riippumatta olosuhteiden vaihtelusta. Tästä syystä aurinkopaneeleihin liitettyjen tehoelektronisten muuttajien ohjauksessa käytetään aina jonkinlaista maksimitehopisteen seurantaa (MPPT, maximum power point tracking).

Viime vuosikymmenten aikana on julkaistu useita MPPT-menetelmiä. Tässä diplomityössä tarkastellaan ja analysoidaan näitä menetelmiä. Kolmeksi parhaiten suuriin ja keskisuuriin aurinkovoimasovelluksiin soveltuviksi algoritmeiksi havaittiin poikkeuta ja havaitse -menetelmä, inkrementaalinen konduktanssi -menetelmä sekä sumea säätö. Näitä kolmea menetelmää vertailtiin ja niiden dynaamista suorituskykyä tarkasteltiin hiljattain julkaistun standardin pohjalta. Työssä esitetään kahteen ensin mainittuun menetelmään useita parannuksia, joilla niiden heikkoa suorituskykyä jatkuvissa muutostiloissa voitaisiin parantaa.

Dynaamisen MPPT-hyötysuhteen testaaminen vaatii pitkiä simulointiaikoja ja paljon muistia, mikäli käytetään yksityiskohtaisia malleja tehoelektronisista muuttajista. Tämä ongelma ratkaistiin laatimalla yksinkertaistettu malli aurinkoenergiajärjestelmästä. Tämä malli validoitiin simuloimalla.

Avainsanat: Aurinkoenergia, maksimitehopisteen seuraaja, poikkeuta ju havaitse, inkrementaalinen konduktanssi, sumea logiikka

Preface

This thesis has been conducted at the Power Electronic Unit in the Department of Electrical Engineering of the Faculty of Electronics, Communications and Automation of Aalto University School of Science and Technology. I would like to acknowledge all the people and institutions that have contributed directly and indirectly in this work.

First of all, I would like to express my gratitude to my supervisor, Prof. Seppo Ovaska for giving me the opportunity of working under his supervision. To Dr. Konstantin Kostov, instructor of this thesis: it would have not been possible to complete this work without his invaluable guidance, advice and support. I have learnt a lot from him during the realization of this thesis.

I am also grateful to my colleagues Lauri Syvaranta and Raúl García Bravo. They have provided me some valuable information for my work and have contributed to the good atmosphere in the office we have been working together.

I would like to thank to William Martin, who have proofread this work, to Jenni Tulensalo, who have help me with the administrative paperwork before and during my stay in Finland and to Jesús A. Oliver, who has supervised my work from my home university in Madrid.

I would like to express thanks to both my home university, Universidad Politécnica de Madrid - Escuela Técnica Superior de Ingenieros Industriales, and Aalto University School of Science and Technology for giving me the opportunity of being an exchange student and even extend the exchange period so that I could finish this thesis in Finland.

And last but not least, to my family, who have encouraged, motivated and supported me during these incredible 16 months I have spent in this lovely country, Finland.

Otaniemi, 14.12.2010

David Sanz Morales

Contents

Abbreviations

AC	Alternate Current
A.M	Air Mass coefficient
CdTe	Cadmium Telluride
CdS	Cadmium Sulphide
CIGS	Copper Indium Gallium (di)selenide
DC	Direct Current
DSP	Digital Signal Processor
ESR	Equivalent Series Resistance
FIS	Fuzzy Inference System
FLC	Fuzzy Logic Control
GaAs	Gallium Arsenide
InCond	Incremental Conductance
LCD	Liquid Crystal Display
MF	Membership Function
MPP	Maximum Power Point
MPPT	Maximum Power Point Tracking
NN	Neural Network
P&O	Perturb and Observe
PV	Photovoltaic
R&D	Research and Development
STC	Standard Test Conditions

Symbols

A	Diode quality (ideality) factor
FF	Fill factor
I	Output current of the PV cell/array
I_0	Dark generated current
I_L	Light generated current
I_{MPP}	Current at the MPP
I_{SC}	Short circuit current
k	Boltzmann's constant
n_p	Number of solar cells connected in parallel
n_s	Number of solar cells connected in series
q	Charge of an electron
R_S	Series resistance of a solar cell
R_{SH}	Shunt resistance of a solar cell
S	Irradiation in W/m^2
T	Absolute temperature
V	Output voltage of the PV cell/array
V_{MPP}	Voltage at the MPP
V_{OC}	Open circuit voltage
ΔI	Increment in the output current of a solar cell/array
ΔP	Increment in the output power of a solar cell/array
ΔV	Increment in the output voltage of a solar cell/array
ΔV_{ref}	Increment in the reference voltage of a solar cell/array

Introduction

Global warming and energy policies have become a hot topic on the international agenda in the last years. Developed countries are trying to reduce their greenhouse gas emissions. For example, the EU has committed to reduce the emissions of greenhouse gas to at least 20% below 1990 levels and to produce no less than 20% of its energy consumption from renewable sources by 2020 [1]. In this context, *photovoltaic* (PV) power generation has an important role to play due to the fact that it is a green source. The only emissions associated with PV power generation are those from the production of its components. After their installation they generate electricity from the solar irradiation without emitting greenhouse gases. In their lifetime, which is around 25 years, PV panels produce more energy than that for their manufacturing [2]. Also they can be installed in places with no other use, such as roofs and deserts, or they can produce electricity for remote locations, where there is no electricity network. The latter type of installations is known as off-grid facilities and sometimes they are the most economical alternative to provide electricity in isolated areas. However, most of the PV power generation comes from grid-connected installations, where the power is fed in the electricity network. In fact, it is a growing business in developed countries such as Germany which in 2010 is by far the world leader in PV power generation followed by Spain, Japan, USA and Italy [3]. On the other hand, due to the equipment required, PV power generation is more expensive than other resources. Governments are promoting it with subsidies or feed-in tariffs, expecting the development of the technology so that in the near future it will become competitive [3]-[4]. Increasing the efficiency in PV plants so the power generated increases is a key aspect, as it will increase the incomes, reducing consequently the cost of the power generated so it will approach the cost of the power produced from other sources.

The efficiency of a PV plant is affected mainly by three factors: the efficiency of the PV panel (in commercial PV panels it is between 8-15% [3]), the efficiency of the inverter (95-98 % [5]) and the efficiency of the *maximum power point tracking* (MPPT) algorithm (which is over 98% [6]). Improving the efficiency of the PV panel and the

inverter is not easy as it depends on the technology available, it may require better components, which can increase drastically the cost of the installation. Instead, improving the tracking of the *maximum power point* (MPP) with new control algorithms is easier, not expensive and can be done even in plants which are already in use by updating their control algorithms, which would lead to an immediate increase in PV power generation and consequently a reduction in its price.

MPPT algorithms are necessary because PV arrays have a non linear voltage-current characteristic with a unique point where the power produced is maximum [7]. This point depends on the temperature of the panels and on the irradiance conditions. Both conditions change during the day and are also different depending on the season of the year. Furthermore, irradiation can change rapidly due to changing atmospheric conditions such as clouds. It is very important to track the MPP accurately under all possible conditions so that the maximum available power is always obtained.

In the past years numerous MPPT algorithms have been published [8]. They differ in many aspects such as complexity, sensors required, cost or efficiency. However, it is pointless to use a more expensive or more complicated method if with a simpler and less expensive one similar results can be obtained. This is the reason why some of the proposed techniques are not used.

Measuring the efficiency of MPPT algorithms has not been standardized until the European Standard EN 50530 was published at the end of May, 2010 [9]. It specifies how to test the efficiency of MPPT methods both statically and dynamically. In any case, there are no publications comparing the results of the different MPPT algorithms under the conditions proposed in the standard.

The objective of this thesis is firstly to review different MPPT algorithms. Then the most popular, *perturb and observe* (P&O), *incremental conductance* (InCond) and *fuzzy logic control* (FLC) are analyzed in depth and tested according to the standard mentioned above. After that, improvements to the P&O and the InCond algorithms are suggested to succeed in the MPP tracking under conditions of changing irradiance. To test the MPPT algorithms according to the irradiation profiles proposed in the standard,

a simplified model was developed, because the simulation time required in some of the cases cannot be reached with the detailed switching model of a power converter in a normal desktop computer. The reason for that is that the computer runs out of memory after simulating only a few seconds with the complete model. Finally, the simplified model is verified by comparing its results with those obtained from a model containing a detailed model of an inverter.

This thesis can be interesting to readers looking for a deeper knowledge in MPP tracking or those looking for an introduction to PV power generation, because it includes a review of the general concepts related to PV power generation.

1 Solar Cell

1.1 Operating principle

Solar cells are the basic components of photovoltaic panels. Most are made from silicon even though other materials are also used.

Solar cells take advantage of the photoelectric effect: the ability of some semiconductors to convert electromagnetic radiation directly into electrical current. The charged particles generated by the incident radiation are separated conveniently to create an electrical current by an appropriate design of the structure of the solar cell, as will be explained in brief below. For further details, the reader can consult references [4] and [10].

A solar cell is basically a p-n junction which is made from two different layers of silicon doped with a small quantity of impurity atoms: in the case of the n-layer, atoms with one more valence electron, called donors, and in the case of the p-layer, with one less valence electron, known as acceptors. When the two layers are joined together, near the interface the free electrons of the n-layer are diffused in the p-side, leaving behind an area positively charged by the donors. Similarly, the free holes in the p-layer are diffused in the n-side, leaving behind a region negatively charged by the acceptors. This creates an electrical field between the two sides that is a potential barrier to further flow. The equilibrium is reached in the junction when the electrons and holes cannot surpass that potential barrier and consequently they cannot move. This electric field pulls the electrons and holes in opposite directions so the current can flow in one way only: electrons can move from the p-side to the n-side and the holes in the opposite direction. A diagram of the p-n junction showing the effect of the mentioned electric field is illustrated in Figure 1.
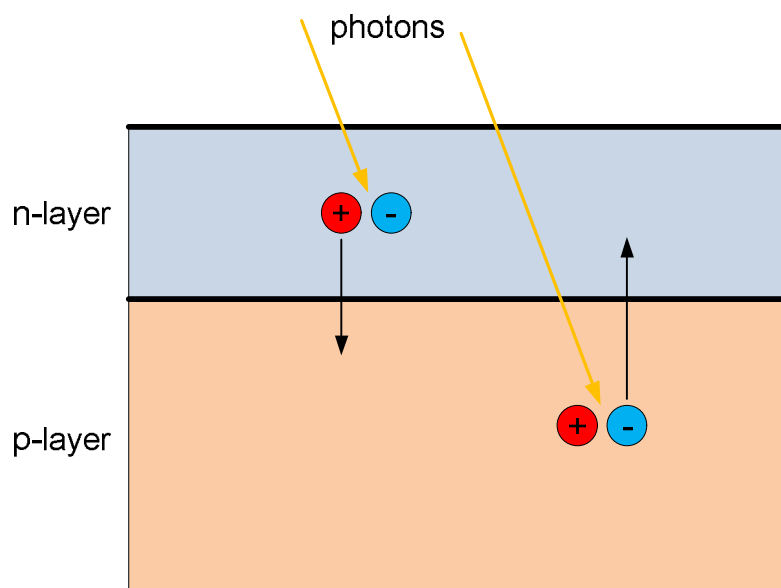
Figure 1 - Solar cell.

Metallic contacts are added at both sides to collect the electrons and holes so the current can flow. In the case of the n-layer, which is facing the solar irradiance, the contacts are several metallic strips, as they must allow the light to pass to the solar cell, called fingers.

The structure of the solar cell has been described so far and the operating principle is next. The photons of the solar radiation shine on the cell. Three different cases can happen: some of the photons are reflected from the top surface of the cell and metal fingers. Those that are not reflected penetrate in the substrate. Some of them, usually the ones with less energy, pass through the cell without causing any effect. Only those with energy level above the band gap of the silicon can create an electron-hole pair. These pairs are generated at both sides of the p-n junction. The minority charges (electrons in the p-side, holes in the n-side) are diffused to the junction and swept away in opposite directions (electrons towards the n-side, holes towards the p-side) by the electric field, generating a current in the cell, which is collected by the metal contacts at both sides. This can be seen in the figure above, Figure 1. This is the light-generated current which depends directly on the irradiation: if it is higher, then it contains more photons with

enough energy to create more electron-hole pairs and consequently more current is generated by the solar cell.

1.2 Equivalent circuit of a solar cell

The solar cell can be represented by the electrical model shown in Figure 2. Its current-voltage characteristic is expressed by the following equation (1):

$$I = I_L - I_0 \left(e^{\frac{q(V - IR_S)}{AkT}} - 1 \right) - \frac{V - IR_S}{R_{SH}} \qquad (1)$$

where I and V are the solar cell output current and voltage respectively, I_0 is the dark saturation current, q is the charge of an electron, A is the diode quality (ideality) factor, k is the Boltzmann constant, T is the absolute temperature and R_S and R_{SH} are the series and shunt resistances of the solar cell. R_S is the resistance offered by the contacts and the bulk semiconductor material of the solar cell. The origin of the shunt resistance R_{SH} is more difficult to explain. It is related to the non ideal nature of the p–n junction and the presence of impurities near the edges of the cell that provide a short-circuit path around the junction [4]. In an ideal case R_S would be zero and R_{SH} infinite. However, this ideal scenario is not possible and manufacturers try to minimize the effect of both resistances to improve their products.
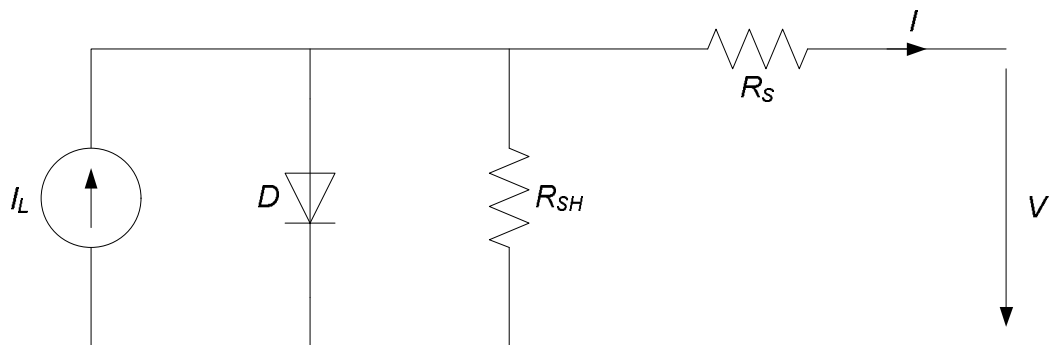

Figure 2 - Equivalent circuit of a solar cell.

Sometimes, to simplify the model, as in [11], the effect of the shunt resistance is not considered, i.e. R_{SH} is infinite, so the last term in (1) is neglected.

A PV panel is composed of many solar cells, which are connected in series and parallel so the output current and voltage of the PV panel are high enough to the requirements of the grid or equipment. Taking into account the simplification mentioned above, the output current-voltage characteristic of a PV panel is expressed by equation (2), where n_p and n_s are the number of solar cells in parallel and series respectively [11].

$$I \approx n_p I_L - n_p I_0 \left(e^{\frac{q(V-IR_S)}{AkTn_s}} - 1 \right) \tag{2}$$

1.3 Open circuit voltage, short circuit current and maximum power point

Two important points of the current-voltage characteristic must be pointed out: the open circuit voltage V_{OC} and the short circuit current I_{SC}. At both points the power generated is zero. V_{OC} can be approximated from (1) when the output current of the cell is zero, i.e. $I=0$ and the shunt resistance R_{SH} is neglected. It is represented by equation (3). The short circuit current I_{SC} is the current at $V = 0$ and is approximately equal to the light generated current I_L as shown in equation (4).

$$V_{OC} \approx \frac{AkT}{q} ln \left(\frac{I_L}{I_0} + 1 \right) \tag{3}$$

$$I_{SC} \approx I_L \tag{4}$$

The maximum power is generated by the solar cell at a point of the current-voltage characteristic where the product VI is maximum. This point is known as the MPP and is unique, as can be seen in Figure 3, where the previous points are represented.
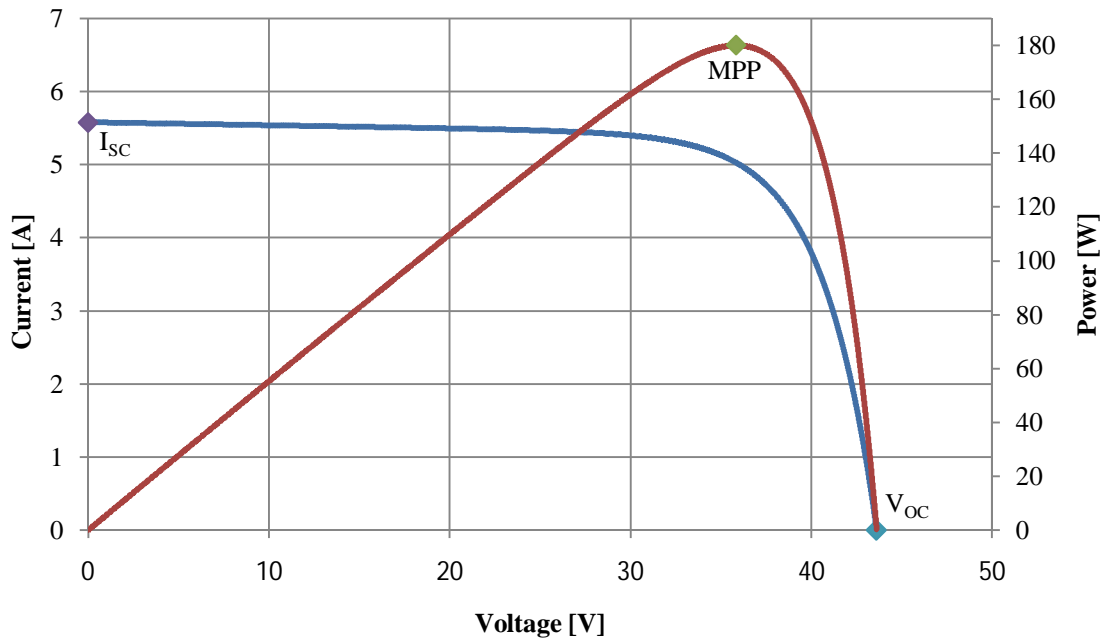
Figure 3 – Important points in the characteristic curves of a solar panel.

1.4 Fill factor

Using the MPP current and voltage, I_{MPP} and V_{MPP}, the *open circuit voltage* (V_{OC}) and the *short circuit current* (I_{SC}), the *fill factor* (*FF*) can be defined as:

$$FF = \frac{I_{MPP}V_{MPP}}{I_{SC}V_{OC}} \tag{5}$$

It is a widely used measure of the solar cell overall quality [4]. It is the ratio of the actual maximum power ($I_{MPP}V_{MPP}$) to the theoretical one ($I_{SC}V_{OC}$), which is actually not obtainable. The reason for that is that the MPP voltage and current are always below the open circuit voltage and the short circuit current respectively, because of the series and shunt resistances and the diode depicted in Figure 2. The typical fill factor for commercial solar cells is usually over 0.70.

1.5 Temperature and irradiance effects

Two important factors that have to be taken into account are the irradiation and the temperature. They strongly affect the characteristics of solar modules. As a result, the

MPP varies during the day and that is the main reason why the MPP must constantly be tracked and ensure that the maximum available power is obtained from the panel.

The effect of the irradiance on the voltage-current (V-I) and voltage-power (V-P) characteristics is depicted in Figure 4, where the curves are shown in per unit, i.e. the voltage and current are normalized using the V_{OC} and the I_{SC} respectively, in order to illustrate better the effects of the irradiance on the V-I and V-P curves. As was previously mentioned, the photo-generated current is directly proportional to the irradiance level, so an increment in the irradiation leads to a higher photo-generated current. Moreover, the short circuit current is directly proportional to the photo-generated current; therefore it is directly proportional to the irradiance. When the operating point is not the short circuit, in which no power is generated, the photo-generated current is also the main factor in the PV current, as is expressed by equations (1) and (2). For this reason the voltage-current characteristic varies with the irradiation. In contrast, the effect in the open circuit voltage is relatively small, as the dependence of the light generated current is logarithmic, as is shown in equation (4).
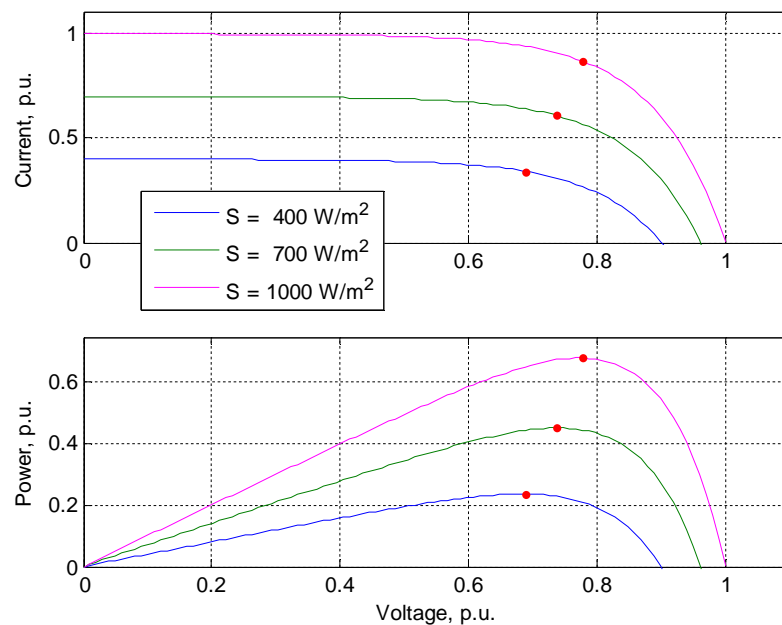

Figure 4 - V-I and V-P curves at constant temperature (25°C) and three different insolation values.

Figure 4 shows that the change in the current is greater than in the voltage. In practice, the voltage dependency on the irradiation is often neglected [10]. As the effect on both

the current and voltage is positive, i.e. both increase when the irradiation rises, the effect on the power is also positive: the more irradiation, the more power is generated.

The temperature, on the other hand, affects mostly the voltage. The open circuit voltage is linearly dependent on the temperature, as shown in the following equation:

$$V_{OC}(T) = V_{oc}^{STC} + \frac{K_{V,\%}}{100}(T - 273.15) \qquad (6)$$

According to (6), the effect of the temperature on V_{OC} is negative, because K_v is negative, i.e. when the temperature rises, the voltage decreases. The current increases with the temperature but very little and it does not compensate the decrease in the voltage caused by a given temperature rise. That is why the power also decreases. PV panel manufacturers provide in their data sheets the temperature coefficients, which are the parameters that specify how the open circuit voltage, the short circuit current and the maximum power vary when the temperature changes. As the effect of the temperature on the current is really small, it is usually neglected [10]. Figure 5 shows how the voltage-current and the voltage-power characteristics change with temperature. The curves are again in per unit, as in the previous case.
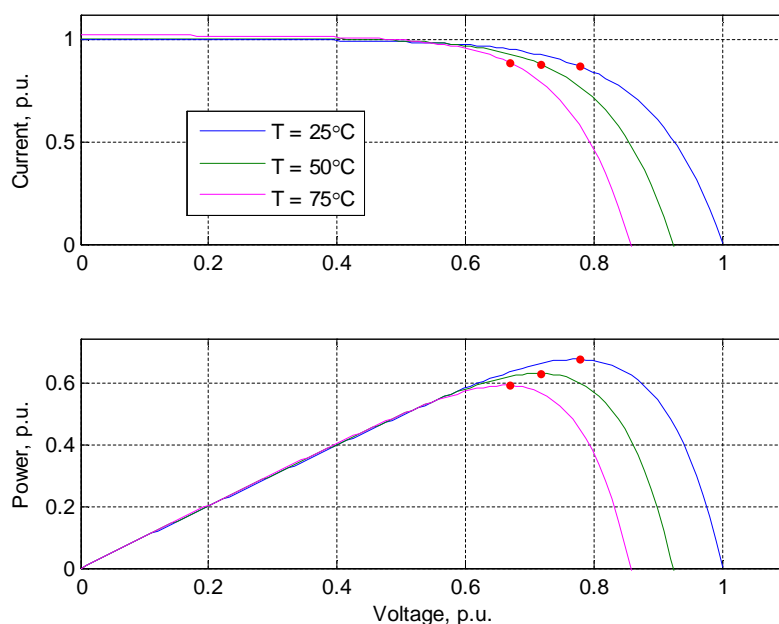

Figure 5 - V-I and V-P curves at constant irradiation (1 kW/m^2) and three different temperatures.

As was mentioned before, the temperature and the irradiation depend on the atmospheric conditions, which are not constant during the year and not even during a single day; they can vary rapidly due to fast changing conditions such as clouds. This causes the MPP to move constantly, depending on the irradiation and temperature conditions. If the operating point is not close to the MPP, great power losses occur. Hence it is essential to track the MPP in any conditions to assure that the maximum available power is obtained from the PV panel. In a modern solar power converter, this task is entrusted to the MPPT algorithms.

1.6   Types of solar cells

Over the past decades, silicon has been almost the only material used for manufacturing solar cells. Although other materials and techniques have been developed, silicon is used in more than the 80% of the production [4]. Silicon is so popular because it is one of the most abundant materials in the Earth's crust, in the form of silicon dioxide, and it is not toxic. Monocrystalline and polycrystalline silicon solar cells are the two major types of silicon solar cells. There is a third type, amorphous silicon, but the efficiency is worse than with the previous types so it is less used. Other new solar cells are made of *copper indium gallium (di)selenide* (CIGS) or *cadmium telluride* (CdTe). Much *research and development* (R&D) effort is being made to develop new materials, but nowadays there are no commercial substitutes to the above types of solar cells. In this section these different solar cells are reviewed.

One of the most important characteristics of solar cells is the efficiency, which is the percentage of solar radiation that is transformed into electricity. It is measured under *Standard Test Conditions* (STC), irradiance of 1000 W/m², air mass coefficient (it characterizes the solar spectrum after the solar radiation has travelled through the atmosphere) A.M 1.5, and a cell junction temperature of 25°C. The higher efficiency, the smaller surface is needed for a given power. This is important because in some applications the space is limited and other costs and parameters of the installation depend on the installed PV surface.

1.6.1 Monocrystalline silicon

Monocrystalline silicon solar cells are the most efficient ones. They are made from wafers (very thin slices) of single crystals obtained from pure molten silicon. These single crystal wafers have uniform and predictable properties as the structure of the crystal is highly ordered. However the manufacturing process must be really careful and occurs at high temperatures, which is expensive. The efficiency of these cells is around 15-18% [3] and the surface needed to get 1 kW in STC is about 7 m^2.

1.6.2 Polycrystalline silicon

These cells are also made from wafers of pure molten silicon. However, the crystal structure is random: as the silicon cools, it crystallizes simultaneously in many different points producing an irregular structure: crystals of random sizes, shapes and orientation. These structures are not as ideal as in the monocrystalline cells so the efficiency is lower, around 11-15% [3]. However the manufacturing process is less expensive, so the lower efficiency is compensated in some way. The surface needed to obtain 1 kW in STC is about 8m^2.

1.6.3 Amorphous and thin-film silicon

Amorphous silicon is the non-crystalline form of the silicon and it can be deposited as thin-films onto different substrates. The deposition can be made at low temperatures. The manufacturing process is simpler, easier and cheaper than in the crystalline cells. The weak point of these cells is their lower efficiency, around 6-8% [3]. This efficiency is measured under STC. However, the performance under weaker or diffuse irradiation, such as that in cloudy days, can be higher than in crystalline cells and their temperature coefficient is smaller [4]. Amorphous silicon is also a better light absorber than crystalline, so despite having low efficiency, the thin film is a competitive and promising technology. The first solar cells were of thin-film technology. They have been used since the 1980s in consumer electronics applications, such as calculators. In recent years it has also begun to be used in high power applications due to the characteristics mentioned above. One common use nowadays is as building cladding,

for example in facades, as its price is competitive compared with other high quality cladding materials and it offer the advantage of electricity generation.

The main advantages of thin film technologies are the ease of manufacturing at low temperatures using inexpensive substrates and continuous production methods, avoiding the need for mounting individual wafers and the potential for lightweight and flexible solar cells. These advantages are common to most of the thin-film solar cells, not only the ones made from amorphous silicon.

Over recent years, one more type of silicon has been developed, microcrystalline silicon [4]. It can also be deposited as thin-films onto different substrates, minimizing the quantities of crystalline silicon needed and improving the efficiency of amorphous silicon. However, the light absorption of microcrystalline silicon compared to amorphous silicon is poor. The solution can be an effective light trapping to keep the incident light within the film. This type of silicon is not a commercial technology yet and more R&D is needed.

1.6.4   Other cells and materials

As was mention in the introduction of this chapter, there are other materials apart from silicon that can be used for manufacturing solar cells. These compounds are also thin-film deposited, so they have the same advantages as the silicon thin film solar cells but with a better efficiency. Among these compounds, two are already used in commercial solar cells. They are CIGS and CdTe. The efficiency is around 10-13% [3] and it will rise in the following years as the technologies are improved. It is commonly said that thin film technology is the way to achieve the grid parity, i.e. the point at which the cost of generating electricity is equal, or cheaper than grid power [4].

The main disadvantages of these technologies are the toxicity of some of the compounds and the shortage of some of the elements used. In the case of the CIGS, indium is used. This element is not as abundant as silicon in the Earth's crust and it is in high demand for other electronics products such as *liquid-crystal display* (LCD) monitors, which has generated a shortage and consequently a high price rise in the

recent years. Moreover, to create the p-n junction, CIGS is interfaced with *cadmium sulphide* (CdS), another semiconductor. The problem is that cadmium is a heavy metal which is cumulatively poisonous. In the case of CdTe, the other compound used in commercial thin film solar cells, it is not as toxic as its individual components, but some precautions must be taken during the manufacturing process.

Gallium Arsenide (GaAs) has been used for space applications mainly for two reasons: firstly, it is less susceptible to suffer damage from the space radiation than silicon, and secondly, due to its direct bandgap of 1.42 eV, it can take advantage of a greater part of the solar spectrum. Despite being a more expensive material, space projects can afford it as cost is not the most important factor to decide the components. Nowadays it is being investigated to be used in terrestrial PV applications using light concentrators (mirror or lenses) to focus the light onto small cells, reducing the price as less material is required. Triple junction GaAs cells have already passed 40% efficiency in the laboratory using light concentrators [4]. The main handicap at present for this technology is that concentration systems are expensive as they have to track the Sun along the day.

One other technology that is being actively researched is dye-sensitized cells [4]. These cells are made from artificial organic materials and are seen as part of the *"third generation"* of solar cells. The efficiency of these cells is above that of amorphous silicon and within the thin-film ones. The main advantage is that they work well under low and diffuse light and their temperature coefficients are lower. The materials used are non-toxic and abundant and their manufacturing processes are relatively simple. Flexible modules can easily be made using flexible substrates and they can be used for building integrated PV: roofs, windows, as they can be manufactured in many shapes, sizes and design criteria.

These last two paragraphs illustrate technologies that are being currently investigated. They are non commercial technologies yet, but it is expected that in the following years they will become competitive and will be also used, increasing the possibilities of PV power generation. The silicon and thin film solar cells described before are currently the technologies used in commercial PV applications.

Nevertheless, what is important for this work is that all the different solar cells presented above have similar non-linear voltage-current characteristics and are affected by irradiation and temperature in a similar way. The only difference is that different type of cells have different levels of sensitivity, nevertheless the same algorithms can be used to track the MPP.

1.6.5   Photovoltaic modules

PV modules are made from solar cells connected in series and parallel to obtain the desired current and voltage levels. Solar cells are encapsulated as they have to be weatherproofed and electric connections also have to be robust and corrosion free. The typical construction of a PV module can be seen in Figure 6.
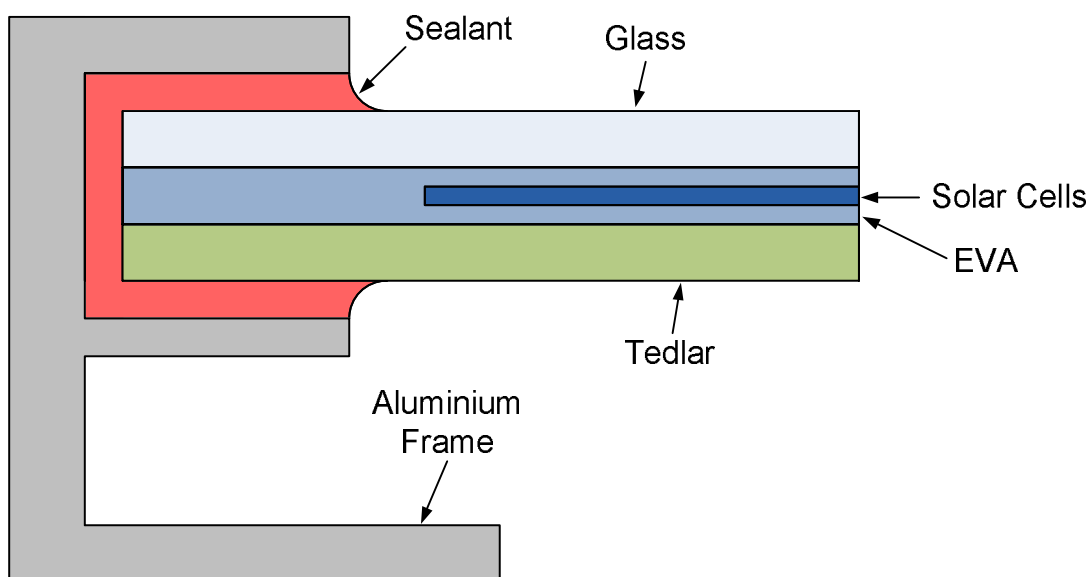

Figure 6 - PV Module typical construction.

As the cells are brittle, they are encapsulated in an airtight layer of *ethylene vinyl acetate* (EVA), a polymer, so the cells are cushioned and in that way are protected during transport and handling. The top cover is a tempered glass treated with an anti-reflection coating so the maximum light is transmitted to the cell. The underneath is a sheet of *polyvinyl fluoride* (PVF), also known as Tedlar, a synthetic polymer $(CH_2CHF)_n$ that constitutes a barrier to moisture and prevents the cell from chemical attack. An aluminium frame is used to simplify mounting and handling and to give extra

protection. Frameless modules are sometimes used in facades for aesthetic reasons. This typical construction is used because the PV module has to "survive" outdoors for at least 20-25 years under different weather conditions, sometimes extreme [4]. This construction assures at least the lifetime of the PV modules. In fact, PV panel manufacturers provide a guarantee of at least 20 years, for example BP Solar assures 85 % of minimum warranted power output after 25 years of service, 93 % of the minimum warranted power output at 12 years and a five-year warranty of materials and workmanship [12]. Such a long guarantee is extremely long compared to most products and is due to the exceptional construction of PV modules.

2 Photovoltaic System Configuration

PV modules generate DC current and voltage. However, to feed the electricity to the grid, AC current and voltage are needed. Inverters are the equipment used to convert DC to AC. In addition, they can be in charge of keeping the operating point of the PV array at the MPP. This is usually done with computational MPP tracking algorithms.

There are different inverter configurations depending on how the PV modules are connected to the inverter [4]. The main types are described in this chapter. The decision on what configuration should be used has to be made for each case depending on the environmental and financial requirements. If the modules are not identical or do not work under the same conditions, the MPP is different in each panel and the resulting voltage-power characteristic has multiple maxima, which constitutes a problem, because most MPPT algorithms converge to a local maximum depending on the starting point. If the operating point is not the MPP, not all the possible power is being fed to the grid. For these reasons each case has to be carefully studied to optimize the plant and obtain the maximum performance.

The different configurations are described shortly in this chapter because they are not the focus of this thesis. More information about all the following topologies can be found in [4] and [13].

2.1 Central inverter

It is the simpler configuration: PV strings, consisting of series connected PV panels, are connected in parallel to obtain the desired output power. The resulting PV array is connected to a single inverter, as is shown in Figure 7. In this configuration all PV strings operate at the same voltage, which may not be the MPP voltage for all of them.

The problem of this configuration is the possible mismatches among the different PV modules. If they are receiving different irradiation (shading or other problems), the true MPP is difficult to find and consequently there are power losses and the PV modules are underutilized.
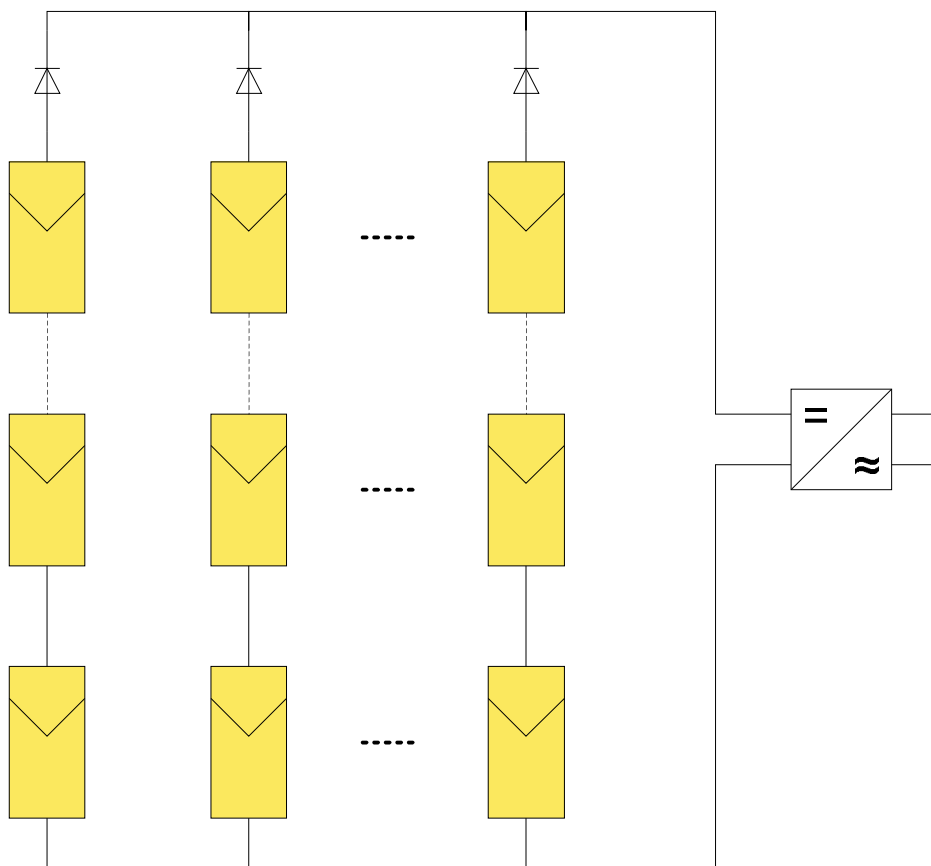
Figure 7 - Central configuration.

2.2   String inverter

In this configuration, every string of PV panels connected in series is connected to a different inverter, as can be seen in Figure 8. This can improve the MPP tracking in case of mismatches or shading, because each string can operate at a different MPP, if necessary, whereas in the central inverter there is only one operating point which may not be the MPP for each string, thus leading to power losses. On the other hand, the number of components of the system increases as well as the installation cost, as an inverter is used for each string.
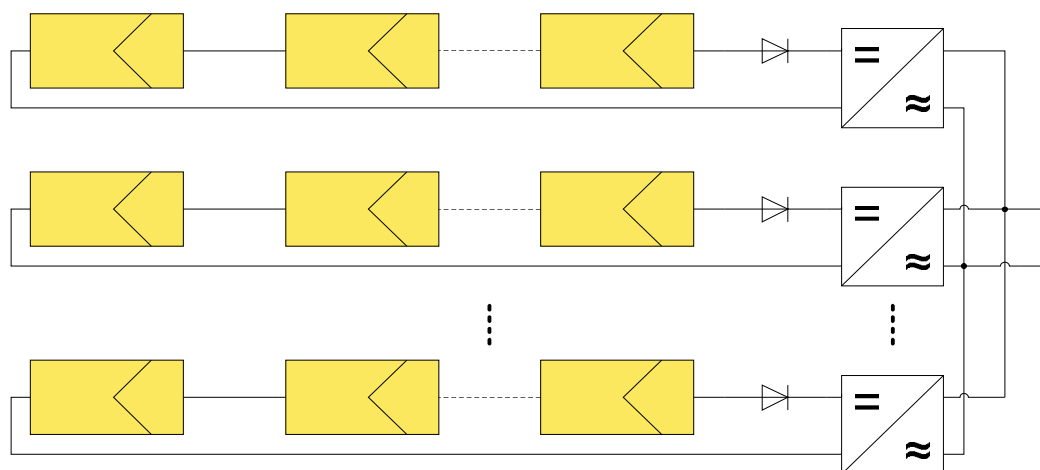
Figure 8 - String configuration.

2.3 Multi-string inverter

In this case each string is connected to a different DC-DC converter, which is in charge of the MPP tracking of the string, and the converters are connected to a single inverter, as depicted in Figure 9. The advantages related to MPP tracking are the same as in the string configuration; each string can have a different MPP. The disadvantages, an increase in the price compared to the central inverter, as a converter is used for each string.

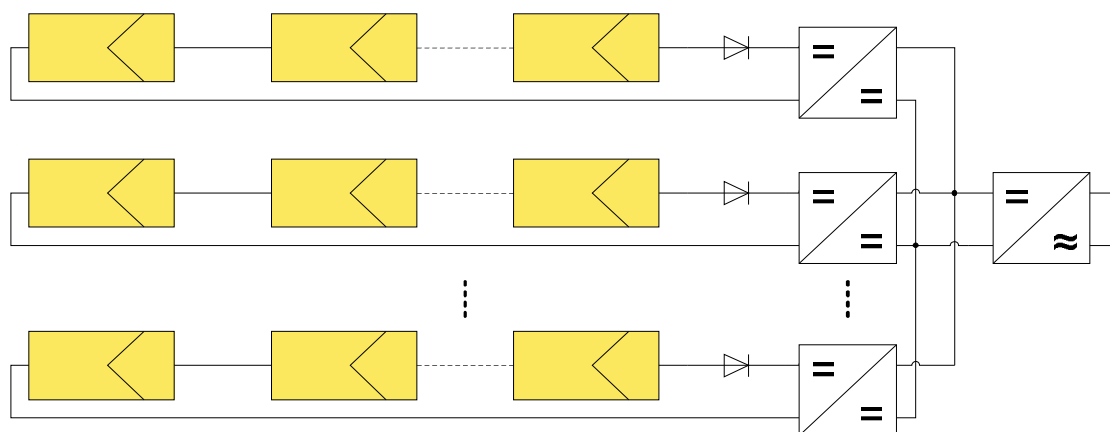
Figure 9 - Multi-string configuration.

2.4 Module integrated inverter

In this configuration, as shown in Figure 10, each PV module is connected to a different inverter and consequently the maximum power is obtained from each panel as the

individual MPP is tracked by each inverter. This configuration can be used when the differences in the operating point of the different modules are large. However, it is more expensive because each panel has its own inverter.
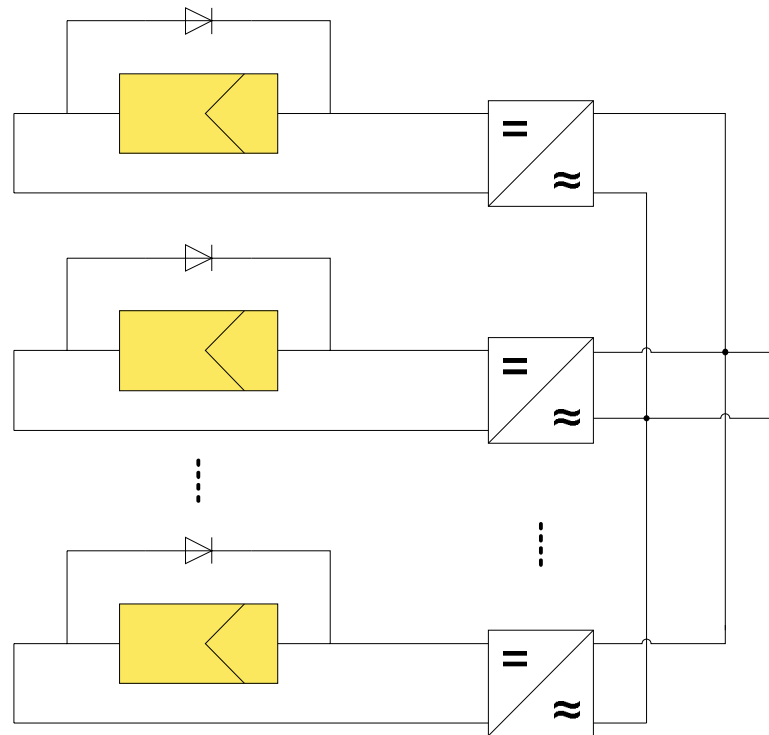

Figure 10 – Individual inverter.

3   Maximum Power Point Tracking Algorithms

As was previously explained, MPPT algorithms are necessary in PV applications because the MPP of a solar panel varies with the irradiation and temperature, so the use of MPPT algorithms is required in order to obtain the maximum power from a solar array.

Over the past decades many methods to find the MPP have been developed and published. These techniques differ in many aspects such as required sensors, complexity, cost, range of effectiveness, convergence speed, correct tracking when irradiation and/or temperature change, hardware needed for the implementation or popularity, among others. A complete review of 19 different MPPT algorithms can be found in [8].

Among these techniques, the P&O and the InCond algorithms are the most common. These techniques have the advantage of an easy implementation but they also have drawbacks, as will be shown later. Other techniques based on different principles are fuzzy logic control, neural network, fractional open circuit voltage or short circuit current, current sweep, etc. Most of these methods yield a local maximum and some, like the fractional open circuit voltage or short circuit current, give an approximated MPP, not the exact one. In normal conditions the V-P curve has only one maximum, so it is not a problem. However, if the PV array is partially shaded, there are multiple maxima in these curves. In order to relieve this problem, some algorithms have been implemented as in [14]. In the next section the most popular MPPT techniques are discussed.

3.1   Hill-climbing techniques

Both P&O and InCond algorithms are based on the "hill-climbing" principle, which consists of moving the operation point of the PV array in the direction in which power increases [14] and [15]. Hill-climbing techniques are the most popular MPPT methods due to their ease of implementation and good performance when the irradiation is constant [15]. The advantages of both methods are the simplicity and low computational

power they need. The shortcomings are also well-known: oscillations around the MPP and they can get lost and track the MPP in the wrong direction during rapidly changing atmospheric conditions [7], [15]-[20]. These drawbacks will be explained later.

3.1.1 Perturb and observe

The P&O algorithm is also called "hill-climbing", but both names refer to the same algorithm depending on how it is implemented. Hill-climbing involves a perturbation on the duty cycle of the power converter and P&O a perturbation in the operating voltage of the DC link between the PV array and the power converter [8]. In the case of the Hill-climbing, perturbing the duty cycle of the power converter implies modifying the voltage of the DC link between the PV array and the power converter, so both names refer to the same technique.

In this method, the sign of the last perturbation and the sign of the last increment in the power are used to decide what the next perturbation should be. As can be seen in Figure 11, on the left of the MPP incrementing the voltage increases the power whereas on the right decrementing the voltage increases the power.
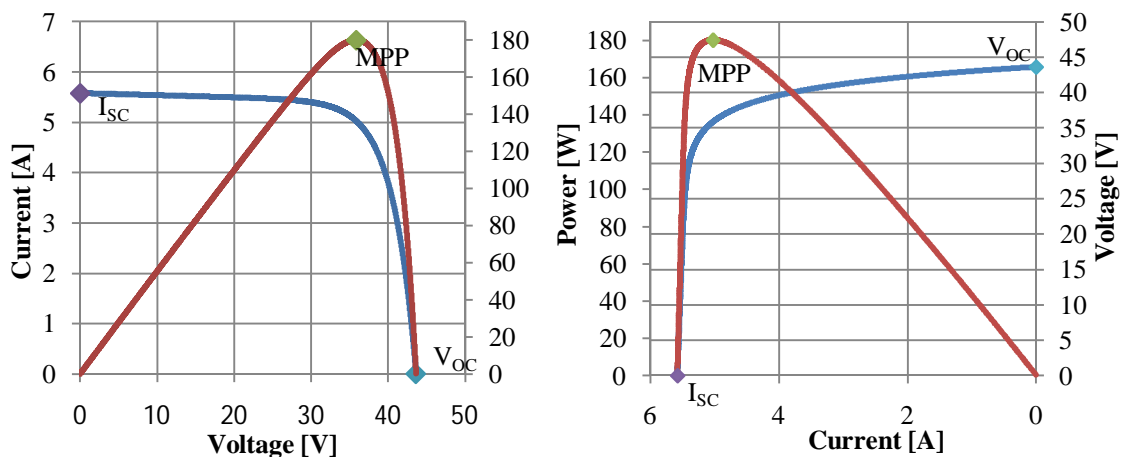

Figure 11- PV panel characteristic curves.

If there is an increment in the power, the perturbation should be kept in the same direction and if the power decreases, then the next perturbation should be in the opposite direction. Based on these facts, the algorithm is implemented [8]. The process is repeated until the MPP is reached. Then the operating point oscillates around the

MPP. This problem is common also to the InCond method, as was mention earlier. A scheme of the algorithm is shown in Figure 12.
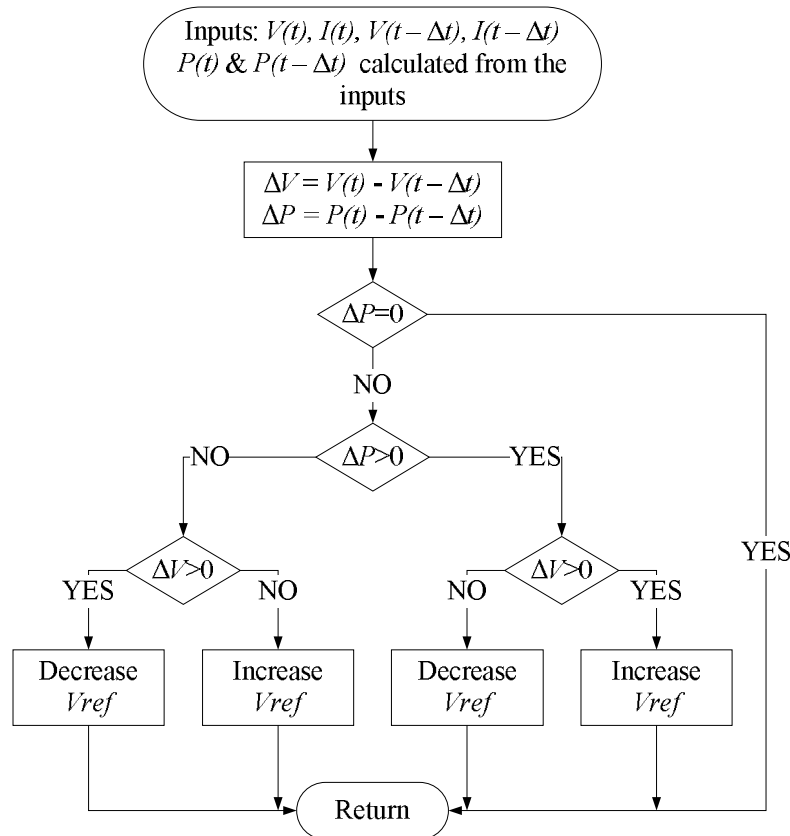

Figure 12 - The flowchart of the P&O Algorithm.

3.1.2 Incremental conductance

The incremental conductance algorithm is based on the fact that the slope of the curve power vs. voltage (current) of the PV module is zero at the MPP, positive (negative) on the left of it and negative (positive) on the right, as can be seen in Figure 11:

- $\Delta V/\Delta P = 0$ ($\Delta I/\Delta P = 0$) at the MPP
- $\Delta V/\Delta P > 0$ ($\Delta I/\Delta P < 0$) on the left
- $\Delta V/\Delta P < 0$ ($\Delta I/\Delta P > 0$) on the right

By comparing the increment of the power vs. the increment of the voltage (current) between two consecutives samples, the change in the MPP voltage can be determined.

A scheme of the algorithm is shown in Figure 13. Similar schemes can be found in [8], [21].
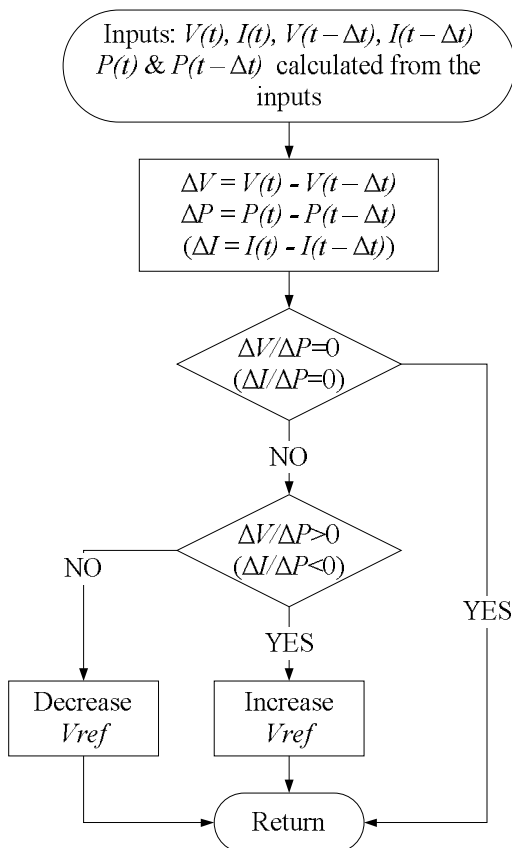

Figure 13 - Incremental Conductance algorithm.

In both P&O and InCond schemes, how fast the MPP is reached depends on the size of the increment of the reference voltage.

The drawbacks of these techniques are mainly two. The first and main one is that they can easily lose track of the MPP if the irradiation changes rapidly [7], [15]-[18]. In case of step changes they track the MPP very well, because the change is instantaneous and the curve does not keep on changing. However, when the irradiation changes following a slope, the curve in which the algorithms are based changes continuously with the irradiation, as can be seen in Figure 14, so the changes in the voltage and current are not only due to the perturbation of the voltage. As a consequence it is not possible for the algorithms to determine whether the change in the power is due to its own voltage increment or due to the change in the irradiation.
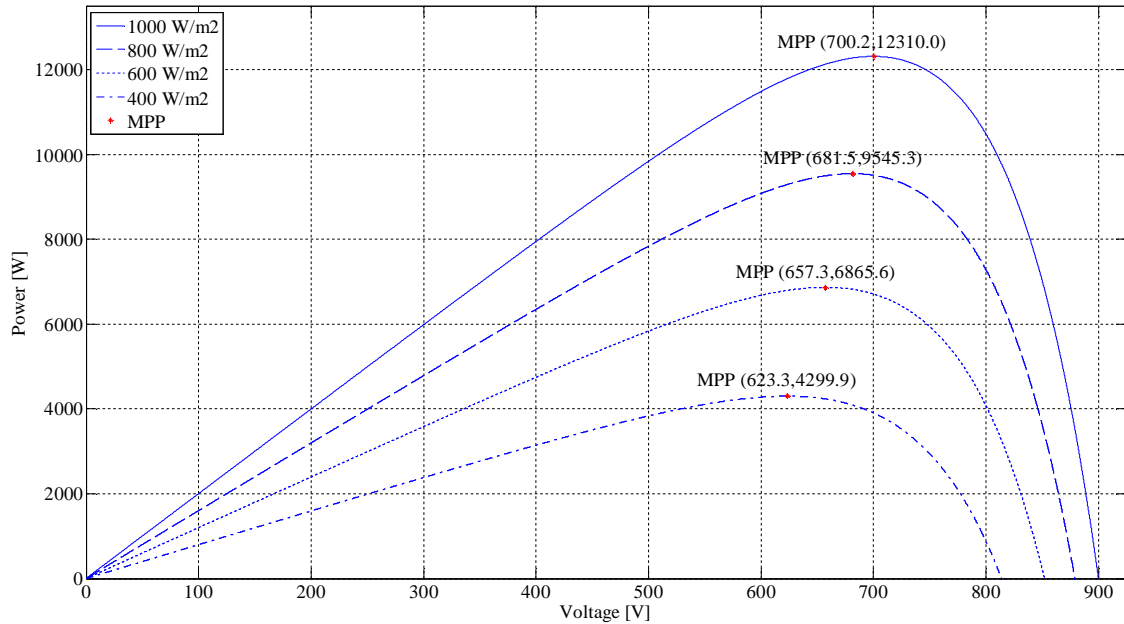
Figure 14 – P-V curve depending on the irradiation.

The other handicap of both methods is the oscillations of the voltage and current around the MPP in the steady state [7], [17], [19] and [20]. This is due to the fact that the control is discrete and the voltage and current are not constantly at the MPP but oscillating around it. The size of the oscillations depends on the size of the rate of change of the reference voltage. The greater it is, the higher is the amplitude of the oscillations. However, how fast the MPP is reached also depends on this rate of change and this dependence is inversely proportional to the size of the voltage increments. The traditional solution is a trade off: if the increment is small so that the oscillations decrease, then the MPP is reached slowly and vice versa, so a compromise solution has to be found.

To overcome these drawbacks some solutions have been published in recent years. Regarding the rapid change of the irradiation conditions, Sera et al. published in [15] and [16] an improved P&O method, called *"dP-P&O"*, in which an additional measurement is performed without perturbation in the voltage and current. In this way, every three consecutive samples the effect of the perturbation in the voltage (current) and the effect of the change in the atmospheric conditions can be evaluated so that the increment in the power used in the algorithm only contains the effect caused purely by

the MPPT algorithm. Then the correct decision about the direction of the next perturbation can be taken. The efficiency of the tracking is improved. Although the method was tested using irradiation slopes, they were not the ones proposed in the new European Standard EN 50530 [9].

A different solution is suggested in [20], which considers the traditional P&O algorithm, in which the perturbation amplitude is tuned constantly taking into account the previous changes in the power. It also includes a stage in which the latest increment in the power is compared with the latest perturbation amplitude to determine if the power increment was due to a change in the irradiation. If this is the case, then the voltage perturbation is set to the same direction as the change in the power condition. The steady state error and the tracking speed are improved, but the algorithm has only been tested with irradiation step changes and not with the irradiation slopes proposed in [9].

In relationship with the oscillations around the MPP in steady state, Zhang et al. proposed in [19] a variable perturbation step for the P&O algorithm to reduce the oscillation around it. This modified P&O method determines also if the operating point is near to or far from the MPP and adjusts the size of the perturbation according to that: if the operating point is near to the MPP, the perturbation size is reduced and if the point is far, then it is increased. This technique improves the convergence speed and reduces the oscillation around the MPP. A similar technique is found in [6]: a variation of the traditional P&O algorithm in which the amplitude of the voltage perturbation is adapted to the actual operating conditions: large perturbation amplitudes are chosen far from the maximum whereas small ones are used near the MPP. The proposed algorithm requires initial panel identification and has to be tuned for each plant. With this technique the dynamic response and the steady state stability are improved. Unfortunately, the last two algorithms do not improve the tracking under changing irradiance conditions. Although the authors claim the performance is better, the algorithms have only been tested with irradiation step changes but not with irradiation ramps as proposed in the European Standard mentioned above [9].

Many papers have been published about optimizing the parameters of these algorithms for different hardware configurations. In [7] the sample frequency for P&O is optimized and in [17] it is shown how the P&O MPPT parameters must be customized to the dynamic behaviour of the specific converter adopted. It has been traditionally said that the performance of InCond algorithm is better than the P&O. However, according to [7] and [17] the performance is similar if the parameters of the P&O method are optimized. In any case, both algorithms are based on the same principle and have the same problem so they have been analyzed together.

The amount of literature presenting slight modifications of the existing methods or adapting them to different hardware configurations is so extensive that it is not possible to present it in this thesis.

In any case, none of the solutions reviewed before solves the problems satisfactorily and none has been tested under the slopes proposed in [9] to test the dynamic efficiency of the MPPT algorithms. These profiles simulate rapid environmental changes such as clouds. It is very important to track the MPP during these situations to obtain the maximum power from the PV module. As will be shown in the next chapter, this thesis proposes some modification to both P&O and InCond methods so that the tracking under irradiation profiles containing slopes is very good.

3.1.3 Other "hill climbing" maximum power point tracking methods

There are other three techniques revised in [8] that can be grouped with the hill-climbing algorithms: *ripple correlation control* (RCC), *dP/dV* or *dP/dI* Feedback control and slide control.

RCC uses the ripple imposed by the power converter on the PV array to track the MPP. It correlates *dp/dt* with *di/dt* or *dv/dt*, to drive the power gradient to zero, which happens when the MPP is reached. According to [22] $\frac{dp}{dt} \cdot \frac{di}{dt}$ or $\frac{dp}{dt} \cdot \frac{dv}{dt}$ are positive to the left of the MPP, negative to the right and zero at the MPP. Actually the same criteria is used by the InCond algorithm but expressed in a different form, thus it will suffer the same problems. In fact, it has been only tested with irradiation steps, which are not

appropriate to test the dynamic performance. Besides, it needs low switching frequencies to have enough ripple so the correct decisions can be made and it is an analog technique. On the contrary, inverters are nowadays controlled digitally with DSPs, so this method does not show any advantage to the P&O or InCond.

dP/dV or *dP/dI* Feedback control is a technique which computes the slope of the P-V or P-I characteristic curve and feeds it back to the controller in order to drive it to zero, as they are zero at the MPP. Again this is another implementation of the InCond algorithm, so it has the same advantages and disadvantages.

Finally, in the slide control, the switching function used is again *dP/dV*, thus the same problems as with the InCond algorithm can be expected under changing irradiation.

To summarise, the last three MPPT methods are based on the same principles as the P&O and the InCond algorithms, so they have the same advantages and disadvantages. All hill-climbing MPPT methods depend on the PV array's V-P or I-P characteristics, which vary with temperature and irradiation, therefore these MPPT methods can be confused when the irradiation or temperature are changing, as it is explained in [15]. Finally, the other hill-climbing MPPT methods do not offer any improvement to the original P&O and InCond algorithms.

3.2   Fuzzy logic control

The use of fuzzy logic control has become popular over the last decade because it can deal with imprecise inputs, does not need an accurate mathematical model and can handle nonlinearity. Microcontrollers have also helped in the popularization of fuzzy logic control [8].

The fuzzy logic consists of three stages: fuzzification, inference system and defuzzification. Fuzzification comprises the process of transforming numerical crisp inputs into linguistic variables based on the degree of membership to certain sets. Membership functions, like the ones in Figure 15, are used to associate a grade to each linguistic term. The number of membership functions used depends on the accuracy of the controller, but it usually varies between 5 and 7 [8], [23]-[25]. In Figure 15 seven

fuzzy levels are used: NB (Negative Big), NM (Negative Medium), NS (Negative Small), ZE (Zero), PS (Positive Small), PM (Positive Medium) and PB (Positive Big). The values *a*, *b* and *c* are based on the range values of the numerical variable. In some cases the membership functions are chosen less symmetric or even optimized for the application for better accuracy [8], [25].
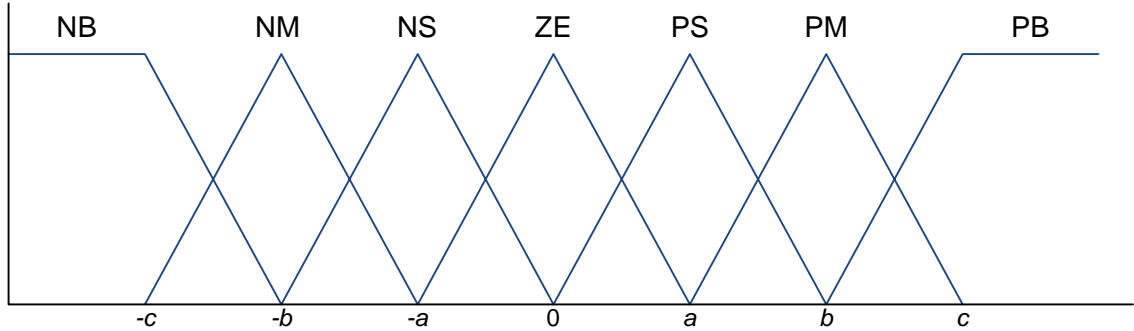

Figure 15 - Membership functions.

The inputs of the fuzzy controller are usually an error, *E*, and the change in the error, ΔE. The error can be chosen by the designer, but usually it is chosen as $\Delta P/\Delta V$ because it is zero at the MPP. Then *E* and ΔE are defined as follows:

$$E = \frac{P(k) - P(k-1)}{V(k) - V(k-1)} \tag{7}$$

$$\Delta E = E(k) - E(k-1) \tag{8}$$

In other cases $\Delta P/\Delta I$ is used as error [23] or other inputs are considered, as in [25], where ΔU and ΔP are used.

The output of the fuzzy logic converter is usually a change in the duty ratio of the power converter, ΔD, or a change in the reference voltage of the DC-link, ΔV. The rule base, also known as rule base lookup table or fuzzy rule algorithm, associates the fuzzy output to the fuzzy inputs based on the power converter used and on the knowledge of the user. Table I shows the rules for a three phase inverter, where the inputs are *E* and ΔE, as defined in (7) and (8), and the output is a change in the DC-link voltage, ΔV. For example, if the operating point is far to the right of the MPP, *E* is NB, and ΔE is zero,

then to reach the MPP the reference voltage should decrease, so ΔV should be NB (Negative) to move the operating point towards the MPP.

Table I - Rule Base.

E\dE	NB	NM	NS	ZE	PS	PM	PB
NB	NB	NB	NB	NB	NM	NS	ZE
NM	NB	NB	NB	NM	NS	ZE	PS
NS	NB	NB	NM	NS	ZE	PS	PM
ZE	NB	NM	NS	ZE	PS	PM	PB
PS	NM	NS	ZE	PS	PM	PB	PB
PM	NS	ZE	PS	PM	PB	PB	PB
PB	ZE	PS	PM	PB	PB	PB	PB

The last stage of the fuzzy logic control is the defuzzification. In this stage the output is converted from a linguistic variable to a numerical crisp one again using membership functions as those in Figure 15. There are different methods to transform the linguistic variables into crisp values. It can be said that the most popular is the center of gravity method. However the analysis of these methods is beyond the scope of this thesis.

The advantages of these controllers, besides dealing with imprecise inputs, not needing an accurate mathematical model and handling nonlinearity, are fast convergence and minimal oscillations around the MPP. Furthermore, they have been shown to perform well under step changes in the irradiation. However, no evidence was found that they perform well under irradiation ramps. Therefore, their performance under the conditions specified in [9] for testing the dynamic MPPT efficiency is unknown. Another disadvantage is that their effectiveness depends a lot on the skills of the designer; not only on choosing the right error computation, but also in coming up with an appropriate rule base [8].

3.3 Neural networks

Another MPPT method well adapted to microcontrollers is Neural Networks [8]. They came along with Fuzzy Logic and both are part of the so called "Soft Computing".

The simplest example of a *Neural Network* (NN) has three layers called the input layer, hidden layer and output layer, as shown in Figure 16. More complicated NN's are built adding more hidden layers. The number of layers and the number of nodes in each layer as well as the function used in each layer vary and depend on the user knowledge. The input variables can be parameters of the PV array such as V_{OC} and I_{SC}, atmospheric data as irradiation and temperature or a combination of these. The output is usually one or more reference signals like the duty cycle or the DC-link reference voltage.
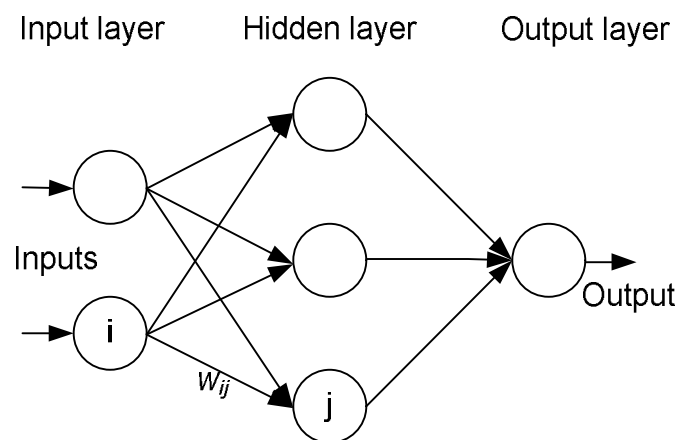

Figure 16 - Neural network.

The performance of the NN depends on the functions used by the hidden layer and how well the neural network has been trained. The links between the nodes are all weighted. In Figure 16 the weight between the nodes *i* and *j* is labelled as w_{ij}. The weights are adjusted in the training process. To execute this training process, data of the patterns between inputs and outputs of the neural network are recorded over a lengthy period of time, so that the MPP can be tracked accurately.

The main disadvantage of this MPPT technique is the fact that the data needed for the training process has to be specifically acquired for every PV array and location, as the characteristics of the PV array vary depending on the model and the atmospheric conditions depend on the location. These characteristics also change with time, so the neural network has to be periodically trained.

3.4   Fractional open circuit voltage

This method uses the approximately linear relationship between the MPP voltage (V_{MPP}) and the open circuit voltage (V_{OC}), which varies with the irradiance and temperature [8]:

$$V_{MPP} \approx k_1 V_{OC} \tag{9}$$

where k_1 is a constant depending on the characteristics of the PV array and it has to be determined beforehand by determining the V_{MPP} and V_{OC} for different levels of irradiation and different temperatures. According to [8] the constant k_1 has been reported to be between 0.71 and 0.78.

Once the constant of proportionality, k_1, is known, the MPP voltage V_{MPP} can be determined periodically by measuring V_{OC}. To measure V_{OC} the power converter has to be shut down momentarily so in each measurement a loss of power occurs. Another problem of this method is that it is incapable of tracking the MPP under irradiation slopes, because the determination of V_{MPP} is not continuous. One more disadvantage is that the MPP reached is not the real one because the relationship is only an approximation.

To overcome these drawbacks, some solutions have been proposed, as is reported in [8]. For example, pilot cells can be used to obtain V_{OC}. They are solar cells that represent the PV array's cells and which are not used to produce electricity but to obtain characteristics parameters such as V_{OC} without interfering with the power converters. These pilot cells have to be carefully chosen and placed to represent the PV array characteristics and the irradiation conditions. One drawback of using these pilot cells is that the cost of the system is increased.

Depending on the application, this technique can be used because it is very easy to implement and it is cheap - it does not require DSP or microcontroller control and just one voltage sensor is used [8]. However, according to [8] this method is not valid under partial shading of the PV array because then the constant k_1 changes. To update then k_1 a

voltage sweep is proposed though this increases the complexity of the system, the cost increases and there are more power losses during the sweep.

3.5   Fractional short circuit current

Just like in the fractional open circuit voltage method, there is a relationship, under varying atmospheric conditions, between the short circuit current I_{SC} and the MPP current, I_{MPP}, as is shown by:

$$I_{MPP} \approx k_2 I_{SC} \qquad (10)$$

The coefficient of proportionality k_2 has to be determined according to each PV array, as in the previous method happened with k_1. According to [8] the constant k_2 has been reported to be between 0.78 and 0.92.

Measuring the short circuit current while the system is operating is a problem. It usually requires adding an additional switch to the power converter to periodically short the PV array and measure I_{SC}. In [26] I_{SC} is measured by shorting the PV array with an additional field-effect transistor added between the PV array and the DC link capacitor. One other option is shown in [27]: a boost converter is used and the switch of the converter is used to short the PV array. Short circuiting the PV array also leads to a loss of power. One last handicap is that the real MPP is not reached because the proportional relationship is an approximation. Furthermore, k_2 changes if the PV array is partially shaded, which happens due to shades or surface contamination. To overcome this problem, [26] proposes an online tuning of k_2 and [28] a periodical sweep of the PV voltage from open circuit to short circuit to update k_2 and guarantee that the real MPP is reached in the presence of multiple maxima which obviously increases the complexity of the system. Most of the literature using this MPPT technique uses a DSP as controller [8].

3.6   Current sweep

In this method the I-V characteristic curve is obtained using a sweep waveform for the PV array current. The sweep is repeated at fixed time intervals so the I-V curve is

updated periodically and the MPP voltage (V_{MPP}) can be determined from it at these same intervals. How the I-V curve is determined and the function chosen for the sweep waveform can be found in [29].

With this method the real MPP is obtained. On the other hand, the sweep takes certain time during which the operating point is not the MPP, which implies some loss of available power. Strictly speaking, it is not possible to track the MPP under irradiation slopes, because the MPP varies continuously. Only if the sweep is instantaneous the global MPP could be found, but that is impossible. Furthermore, the implementation complexity is high, the convergence speed is slow and both voltage and current measurements are required. As pointed out in [29] a MPPT method is worth using only if its power consumption is lower than the increase in power it brings to the entire PV system.

Due to the drawbacks and complexity exposed above, this MPPT method is not the best option to track the MPP continuously. However, it can be used as a complement to other methods, for example when initializing the PV system in the morning, to begin the tracking in the real MPP and then change to another algorithm, or to check sometimes during the day if the system is operating at the real MPP. One more application can be checking if there are multiple maxima due to shading conditions.

3.7 Maximum power point current and voltage computation

I_{MPP} & V_{MPP} computation is a technique in which the MPP is calculated based on the measurements of the irradiance and the temperature using a model of the PV module [8]. The drawbacks are the extra measurements needed, which are sometimes difficult to obtain, and the necessity of an accurate model of the PV array. On the other hand, the MPP is correctly tracked even under changing atmospheric conditions. It can be used in large plants, where the economic investment is huge and a perfect tracking is needed to obtain the maximum available power from the solar arrays.

3.8   State based maximum power point tracking technique

The state based MPP technique is based on a state-space representation of the plant and a nonlinear time-varying dynamic feedback controller. This technique is argued to be robust and tracks the MPP even under changing irradiation and in the presence of multiple maxima. However, no experimental results are given in [30], the implementation complexity is high, as the state-space representation has to be built for each PV plant, and the performance under changing irradiance has not been tested according to the standard.

3.9   Multiple maxima search

It has not been considered in this thesis, but when the PV array is shaded the *P-V* curve presents multiple maxima and most MPPT algorithms including P&O, InCond and fuzzy logic control, cannot determine the global maximum. Usually a local MPP is found, depending on the starting point of the algorithm [14]. In recent years, some algorithms have been proposed to overcome this limitation. The most relevant are reviewed in the introduction of [14], which claims that the most effective is the DIRECT search technique that is based on the dividing rectangles algorithm. If this method is continuously used to track the MPP, the maximum reported efficiency is 97% [14]. However, it can be used periodically to determine where the global maximum is and then change to a traditional algorithm whose efficiency can be over 99% [6].This could be effective as the shades move slowly during the day. In this way, the losses that occur due to convergence to a local instead of the global MPP, which is a handicap of most traditional algorithms, could be avoided.

3.10   Maximum power point tracking summary

Most of the MPPT algorithms developed over the past years have been reviewed in the previous sections. Some of them are very similar and use the same principle but expressed in different ways, like the last three algorithms listed in the hill-climbing techniques.

The most popular MPPT algorithms according to the number of publications are P&O, InCond and Fuzzy Logic. It makes sense because they are the simplest algorithms capable of finding the real MPP. However, they have some disadvantages, as discussed earlier. In the following chapter, the performance of these three algorithms is analyzed. They were selected because of their simplicity and popularity. In the case of P&O and InCond some modifications are proposed, which overcome the limitations of the original methods in tracking the MPP under irradiation slopes. The FLC is designed according to the references and its dynamic efficiency is tested and compared to the hill-climbing MPPT methods.

4 Maximum Power Point Tracking Algorithms Efficiency Tests

4.1 Simulation model

One of the objectives of this thesis is to develop a model to test the dynamic performance of different MPPT algorithms independently of the converter used. Detailed models of the PV system with the switching model of the power converter are computationally very heavy and the time that can be simulated in a normal computer is only a few seconds. However the simulation time required for testing the system with the irradiation profiles proposed in [9] can be up to several minutes, which can be difficult or impossible to achieve on a PC, if a complete model of the PV system is used, because the computer runs out of memory after some seconds are simulated.

The model proposed here was developed in Matlab[®]/Simulink[®] and consists of a model of the PV array, the DC-link capacitor and a controlled current source, which replaces the power converter. The MPPT Control block generates the reference voltage using the MPPT algorithm under test. This model is depicted in Figure 17. The model of the PV array used in this work was designed following the references [31]-[36].
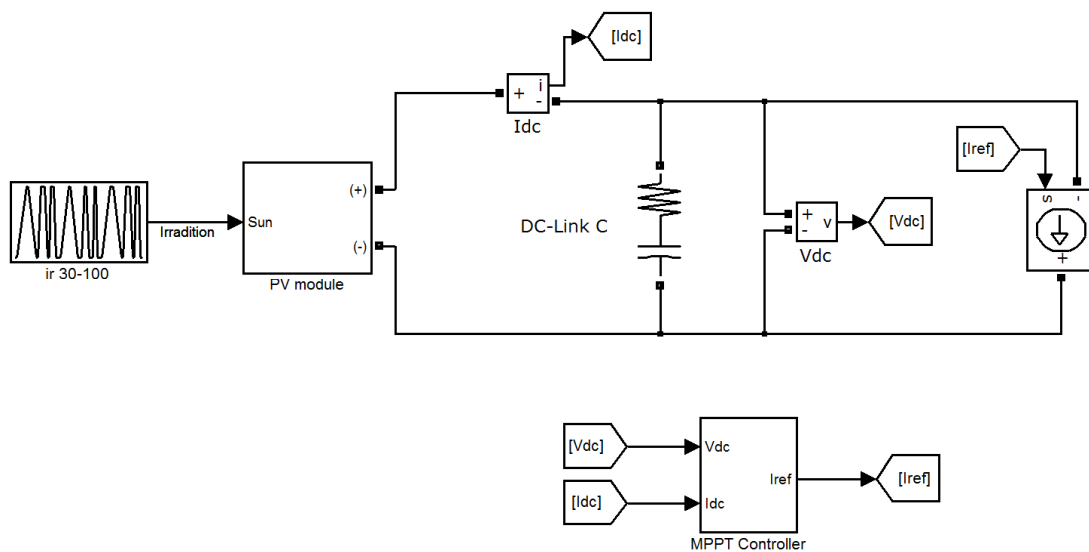

Figure 17 - Model used for simulations.

38

The reference voltage generated by the MPPT Control block is converted to a current reference using the control scheme described in [11] and shown in Figure 18.
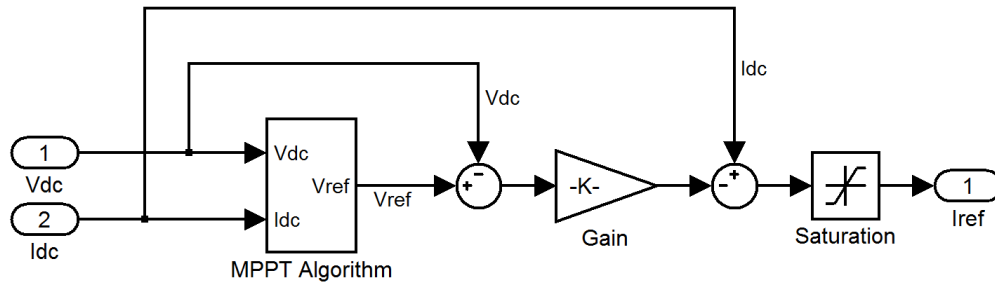

Figure 18 - MPPT Controller.

In this scheme, the error between the reference and the actual DC voltage (the output voltage of the PV array) is fed in a proportional gain, whose value depends on the DC-link capacitance and the sampling period. The output of this gain is subtracted from the current of the PV module and the result is the reference current for the controlled current source.

As the model is simpler the simulation time can be much longer: using a conventional computer, the time needed to simulate 130 seconds is only a few minutes, and the simulation time can be over 1000 seconds. However, if the model includes a detailed switching power converter, for example, a three phase inverter, the simulation time can be only a few seconds and the time needed for MPPT efficiency tests is much longer.

The parameters of the system used in all the simulations performed in this thesis are as follows:
Solar panel characteristics at STC:
- Open circuit voltage: 900 V
- Voltage at MPP: 700.2 V
- Short circuit current: 20 A
- Current at MPP: 17.6 A

DC-Link Capacitor:
- Capacitance: 700 μF
- ESR: 1 mΩ

Sampling frequency:

- MPPT algorithm: 25 Hz
- V and I measurements: 20 kHz

The characteristics of the solar array were chosen in order to fulfil the requirements of the inverter. The input voltage of the inverter (V_{MPP}) has to be greater than the peak line-to-line voltage of the output ($\sqrt{6} \cdot 230V \approx 563V$). The current was selected in order to have a level of power over 10 kW.

The sampling frequency of the MPPT algorithm was selected according to [7] whereas the sampling frequency of the voltage and current measurements was chosen according to the sampling time of a modern DSP. The sample frequency of the MPPT algorithm should not be very high because the dynamics of the weather conditions is slow compared to the dynamics of systems typically studied in control theory.

4.2 Original algorithms

Using the model described in the previous section, first the original P&O and InCond algorithms were dynamically tested. The standard for MPPT efficiency proposes slopes with different gradients as well as different irradiance levels. The gradients vary from 0.5 to 100 W/m^2/s. Two irradiation levels are considered: from low to medium irradiance, 100 to 500 W/m^2, and from medium to high, 300 to 1000 W/m^2. The concrete gradients which must be used in the two cases are shown in Tables II and III respectively [37] and [38].

Table II – Slopes proposed for irradiance levels from 100 to 500 W/m^2.

Slope (W/m^2/s)	Rise time (s)	Dwell time	Total Simulation time
0.50	800.00	10.00	1630.00
1.00	400.00	10.00	830.00
2.00	200.00	10.00	430.00
3.00	133.33	10.00	296.67
5.00	80.00	10.00	190.00
7.00	57.14	10.00	144.29
10.00	40.00	10.00	110.00
14.00	28.57	10.00	87.14
20.00	20.00	10.00	70.00
30.00	13.33	10.00	56.67
50.00	8.00	10.00	46.00

To test the original P&O and InCond algorithms, two different slopes from Table III are chosen: 20 and 100 W/m^2/s. They are enough to demonstrate that the original algorithms based on the hill climbing principle fail under changing irradiance.

Table III - Slopes proposed for irradiance levels from 300 to 1000 W/m^2.

Slope (W/m^2/s)	Rise time (s)	Dwell time	Total Simulation time
10.00	70.00	10.00	170.00
14.00	50.00	10.00	130.00
20.00	35.00	10.00	100.00
30.00	23.33	10.00	76.67
50.00	14.00	10.00	58.00
100.00	7.00	10.00	44.00

4.2.1 Perturb and observe

The algorithm shown in Figure 12 is implemented in the MPPT Algorithm block shown in Figure 18. Two different rates of change of the reference voltage (ΔV_{ref}) are considered: 3 and 1 V. The first slope has a gradient of 20 W/m^2/s and the second one of 100 W/m^2/s. Figure 19 illustrates the results of the test.
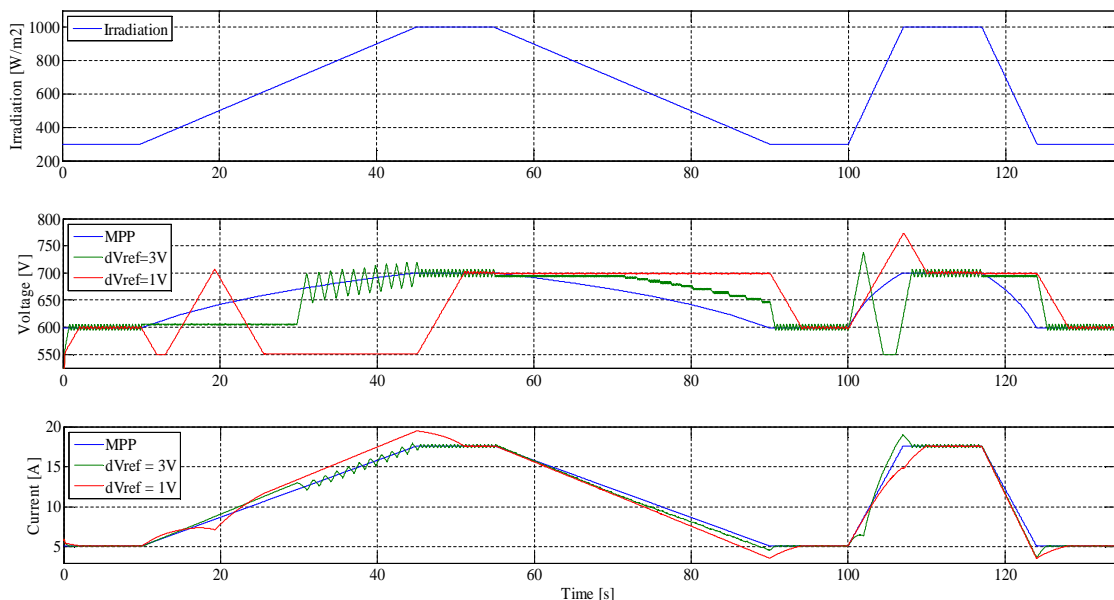
Figure 19 – Performance of the P&O original algorithm under slopes of 20 and 100 W/m^2/s. The MPP values are shown in blue whereas the real values corresponding to the two cases studied, ΔV_{ref} set to 3 and 1 V, are shown in green and red respectively.

As seen in Figure 19, the algorithm cannot track accurately the MPP when the irradiance changes continuously. The PV array voltage in both cases, when ΔV_{ref} is set to 3 V and 1 V, is far from the MPP when the irradiation changes. However, when the irradiation is constant, it oscillates around the MPP value. The amplitude of the oscillations depends directly on the size of the increment in the reference voltage, ΔV_{ref}. Also, when the irradiation is constant, the corresponding MPP voltage is reached after a delay, which depends on the size of ΔV_{ref}. In other words, when ΔV_{ref} is 3V, the oscillations around the MPP are greater but the time to reach the steady state is shorter than in the other case, when ΔV_{ref} is 1V.

Figure 20 depicts the performance of the algorithm under a step. In this case the tracking is adequate, which demonstrates that irradiation step changes do not pose a challenge to the hill-climbing algorithms and are not suitable for testing MPPT. As expected, the convergence speed, i.e. how fast the steady state is reached, and the amplitude of the oscillations are a trade off, as both cannot be improved at the same time: if one is reduced the other increases, because both depend directly on the size of the voltage increment.
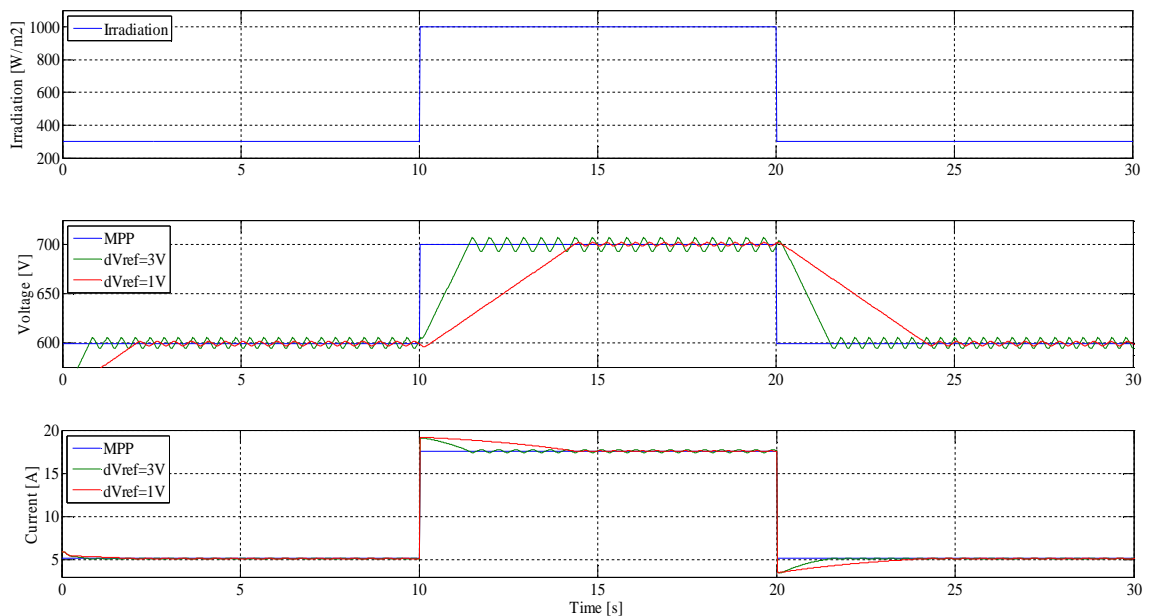

Figure 20 - Performance of the P&O original algorithm under step changes from 300 to 1000 W/m^2.

4.2.2 Incremental conductance

Figure 32 and Figure 33 in Appendix A illustrate the same tests performed with the P&O repeated with the InCond algorithm. The results are practically identical with both methods. The algorithm suffers the same problems under changing irradiance and the same trade-off exists between the convergence speed and the amplitude of the oscillation in steady state.

4.3 Modified algorithms

From the results of the previous tests under irradiation slopes, it is obvious that with both algorithms the voltage from the PV panel is far from the MPP voltage. Moreover, the algorithms may even move the DC voltage in the wrong direction. Interestingly, the current tracks closely the MPP current and in the correct direction. The same can be said about the power, as can be seen in Figure 21.
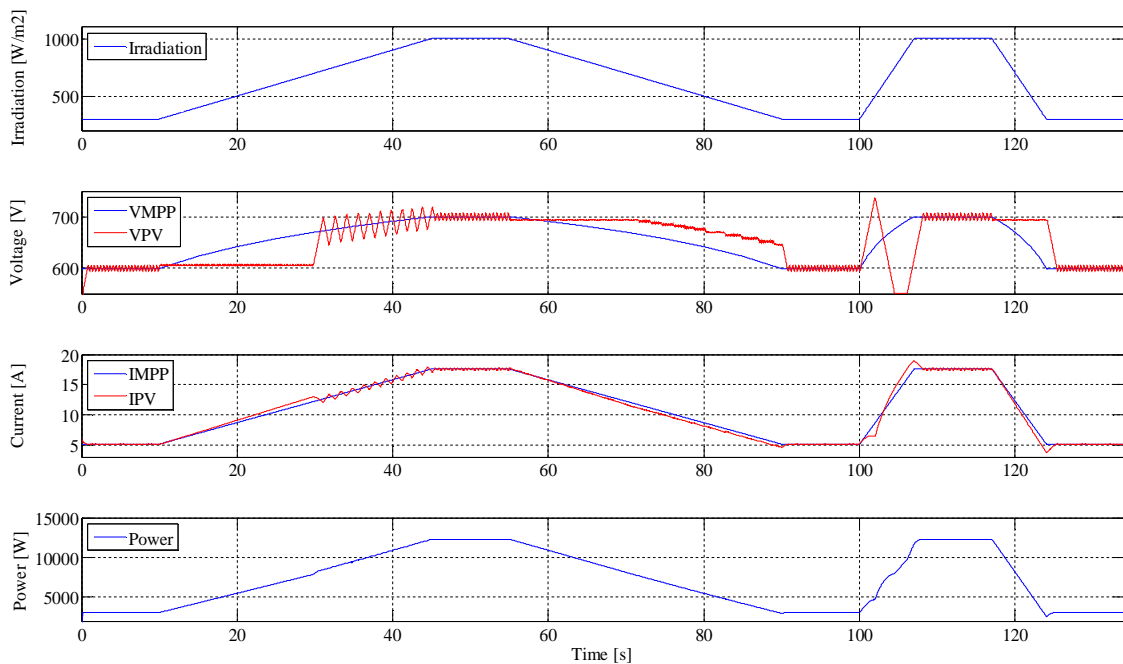
Figure 21 - Voltage, current and power under irradiation ramps.

This is due to the fact that the current of the PV array is directly proportional to the irradiation. For this reason, when the irradiation varies following a slope the PV current has a similar behaviour. In theory, if the current changes linearly, for a given (constant)

sampling frequency, there should be a specific optimal current increment. The power also changes in the same direction as the current does. When the algorithm gets confused, the current and power do not change smoothly, but nevertheless they can be used to determine the direction of the change of the MPP. If the irradiation is increasing following a slope, both the current and power increase and vice versa: if the current decreases, then the current and power decrease.

To track correctly the MPP under irradiation slopes it is necessary to take into account not only the last increment in the current and voltage but at least three, so it can be determined how they are varying over a longer time interval. To do so, four consecutive samples of the voltage and current are taken into account. With them the last three increments in the power (ΔP) and current (ΔI) can be calculated. If the average of the current increments is within an interval around the last increment in the current, in this work it has been used an interval $\pm 20\%$ of the last increment, i.e. ($1.2\Delta I$, $0.8\Delta I$), and the last three increments in the current and power have the same sign, then the irradiation is changing following a slope and the reference voltage is forced to move in the right direction: it is increased if the current is increasing and decreased in the opposite case.

This solution works properly with the P&O. However, using the incremental conductance algorithm, some problems were found when the irradiation changes: they were related to the use of $\Delta V/\Delta P$ or $\Delta I/\Delta P$ to determine V_{ref}. The problem appears in the two following cases: if the irradiation decreases and $\Delta V/\Delta P$ is employed or if $\Delta I/\Delta P$ is used and the irradiation increases. In the first case, ΔP and ΔV are both negative but the sign of $\Delta V/\Delta P$ is positive and the algorithm dictates to increase V_{ref} instead of reducing it, as can be seen in Figure 11. In the second case, ΔP and ΔI are positive and the sign of $\Delta I/\Delta P$ is also positive, so the reference voltage is decreased instead of increased. The solution is simple because the problem only appeared in these two cases: when ΔI is negative, the algorithm makes use of $\Delta I/\Delta P$ and in the other cases $\Delta V/\Delta P$ is utilized. The new flowchart is depicted in Figure 22.
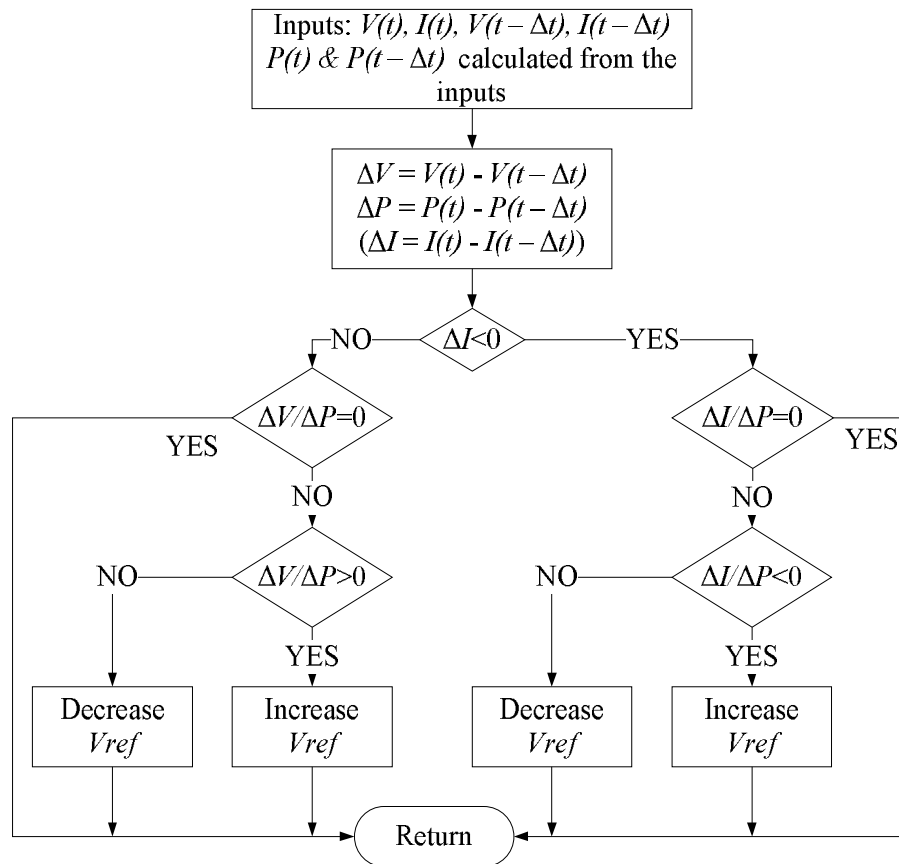
Figure 22 - New flowchart of the InCond algorithm.

After these modifications and using the commands previously explained, the InCond algorithm is also capable of tracking the MPP correctly under changing irradiance. The outcomes of both algorithms are shown later in this section after another modification to the algorithms.

After the confusion of the algorithms under irradiation slopes was overcome, the objective shifted on making the increment in the reference voltage adaptive to the operating point. The reason is that the MPP voltage does not change linearly with time, as seen in Figure 19, and therefore to track the MPP under irradiation slopes, the increment in the reference voltage must change in order to get maximum of the available power. Also a constant increment in the reference voltage would limit the convergence speed and fix the amplitude of the oscillations around the MPP when the irradiation is constant.

It was studied how the MPP voltage and current vary each 5 W/m^2 when the irradiation changes between 100 W/m^2 and 1000W/m^2. Then the increment in the current (ΔI) and voltage (ΔV) between each two consecutive points and the relationship $\Delta I(k)/\Delta V(k)$ were calculated. This relationship is represented versus the PV array current, $I_{dc}(k)$ in Figure 23.
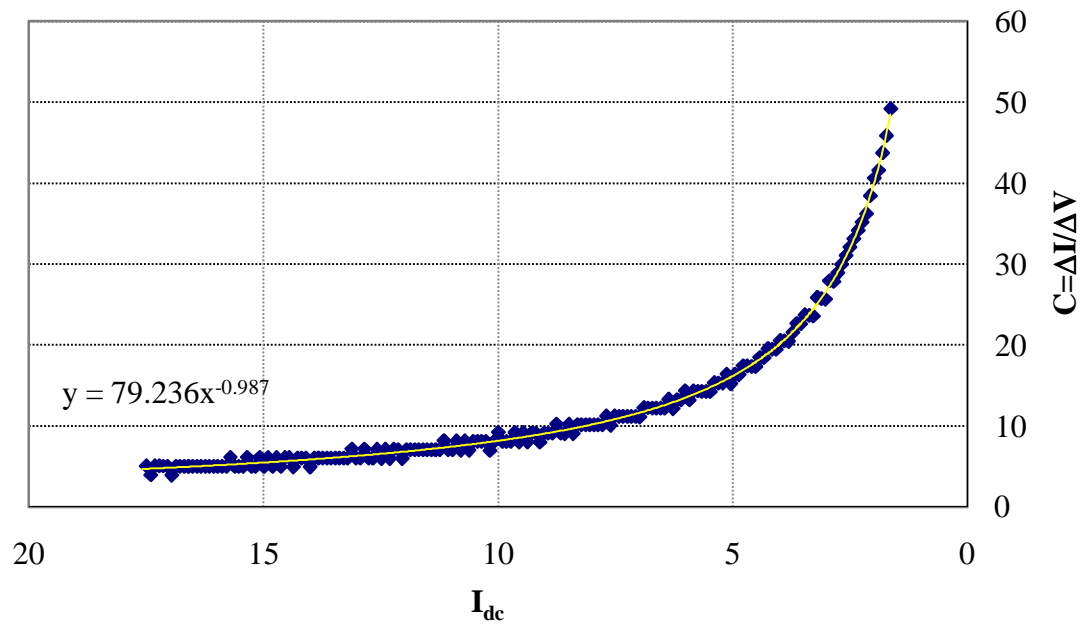

Figure 23 - $\Delta I/\Delta V$ – I_{dc} curve.

The point distribution is approximated by the equation shown in the figure. How the reference voltage should vary to track the MPP can be approximated using the following equation:

$$\Delta V_{ref}(t+1) = 79.236 \cdot I_{dc}(t)^{-0.987} \cdot \left|\Delta I(t)\right| \tag{11}$$

Equation (11) is valid for the PV array used in this work. However, repeating the same process using the characteristics of a different PV array would lead to a similar figure and equation valid for the corresponding PV array. Calculating the size of the voltage perturbation using this method leads to very good tracking under fast irradiation changes.

After the above modifications, it was found that the algorithm did not respond to irradiance step changes. The solution to this problem is to set an increment in the reference voltage greater than the standard value if the increment in the current is large. For example, for a system with the parameters in this Chapter, when ΔI is larger than 0.25 A then ΔV is 9 V. With this simple command the problem was solved.

After the modifications described so far, the algorithm was able to track the MPP voltage under both irradiation slopes and step changes. Finally, the oscillation around the MPP in steady state can be minimized making the change in the reference voltage proportional to the increment in the current. A standard rate of change is fixed (in this case it was 3 V) and if ΔI is smaller than a certain value, then ΔV_{ref} is reduced. In this case six options were considered, which were determined by trial and error, i.e. the values were adjusted until satisfactory performance was achieved. The six cases are:

- If ΔI has oscillated around zero during the latest four samples, then $\Delta V_{ref} = 0.10$ V.
- If ΔI is smaller than 0.001 A, then ΔV_{ref} is 0.05 V.
- If ΔI is smaller than 0.005 A, then ΔV_{ref} is 0.2 V.
- If ΔI is smaller than 0.01A, then ΔV_{ref} is 0.5 V.
- If ΔI is smaller than 0.015 A, then ΔV_{ref} is d/2 (d is the standard value).
- In the rest of the cases, $\Delta V_{ref} = 3$ V (standard value).

With this method the steady-state ripple was almost eliminated, but has to be tune case by case.

All modifications described above can be summarized in the flowchart of in Figure 24. It has the following five stages:

1. Calculation of the power and the increments in the power, voltage and current.
2. Determining the rate of change in the reference voltage by taking into account, first the step changes and then the six cases depending on the value of ΔI.
3. Core algorithm (P&O or InCond as shown in Figure 12 or Figure 22 respectively).

4. Determining the irradiation slope, by comparing the last three increments in the current and power, and adjusting ΔV_{ref} according to (11).

5. Setting limits in the reference voltage so it is within the minimum and maximum input voltages of the converter.

```
┌─────────────────────┐
│   Calculations:     │
│  Power, increments  │
│     in V, I, P      │
└─────────────────────┘
           │
           ▼
┌─────────────────────┐
│  Determine ΔVref    │
│  depending on ΔI    │
└─────────────────────┘
           │
           ▼
┌─────────────────────┐
│  InCond or P&O      │
│    Algorithm        │
└─────────────────────┘
           │
           ▼
┌─────────────────────┐
│  Slopes Tracking    │
│   (if necessary)    │
└─────────────────────┘
           │
           ▼
┌─────────────────────┐
│  Setting Limits in  │
│       Vref          │
└─────────────────────┘
```
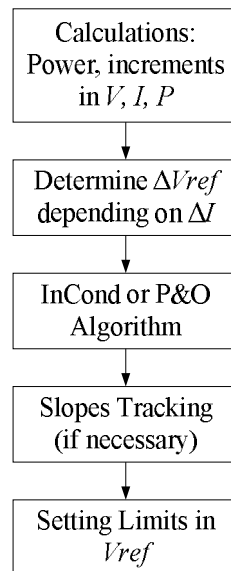
Figure 24 – Flowchart of the proposed modified algorithm.

The performance of the modified algorithm has been tested according to all the slopes proposed in Table II and Table III. Both the P&O and InCond algorithms have been considered in the core of the modified algorithm. Figure 25 and Figure 26 portray the performance of the modified algorithms under irradiation ramps with gradients of 20, 50 and 100 W/m^2/s. The results with the remaining slopes are shown in Appendix A.
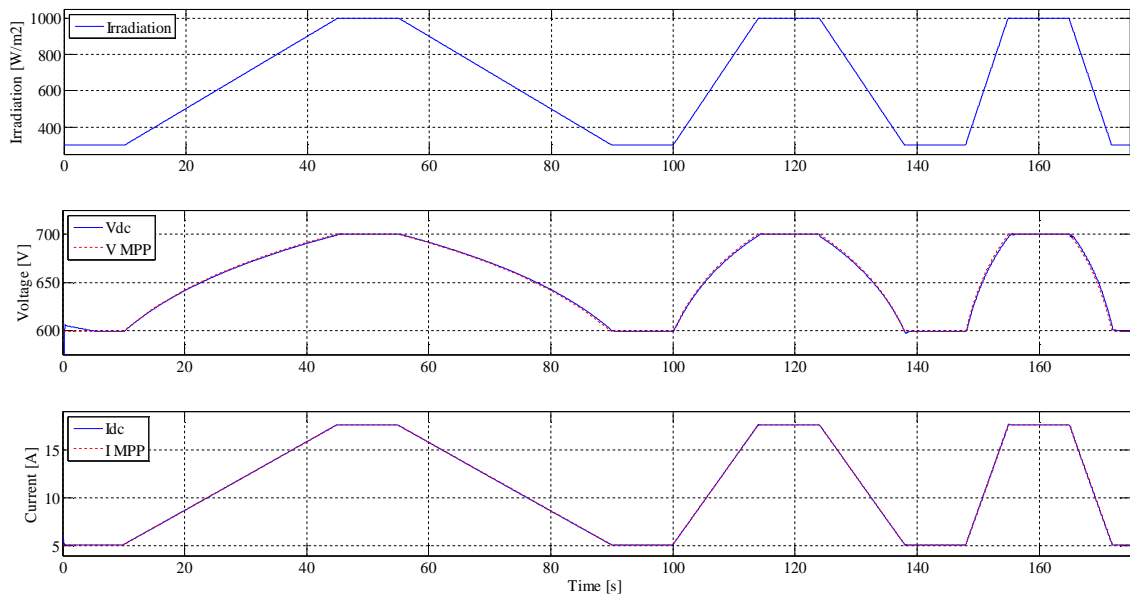
Figure 25 - P&O MPPT algorithm dynamic efficiency test. The algorithm tracks the MPP under the irradiation slopes proposed in the standard.
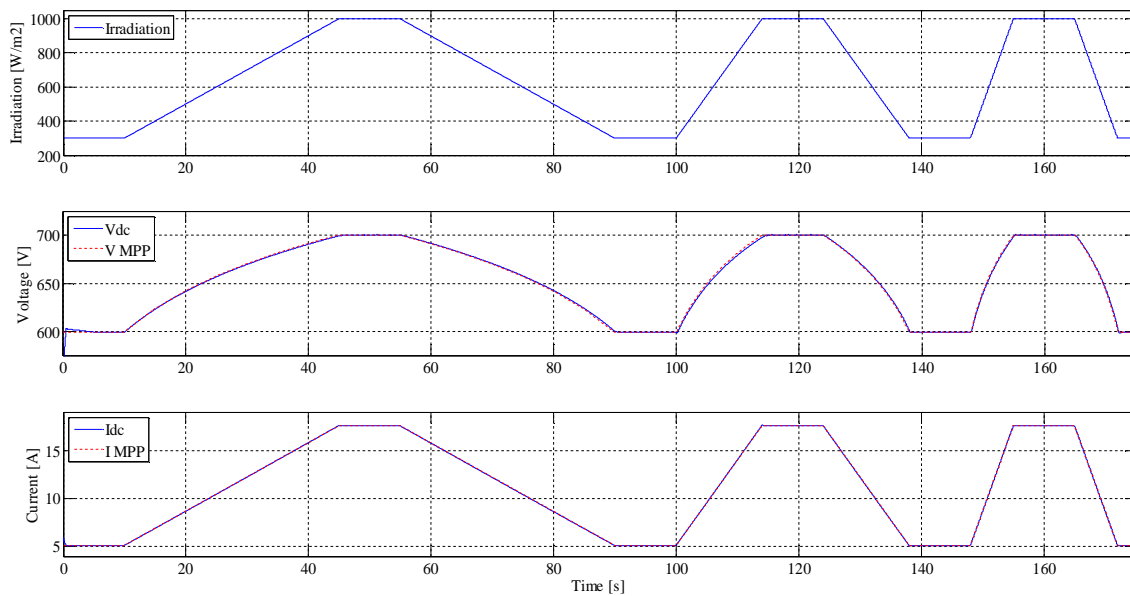

Figure 26 - Incremental Conductance MPPT algorithm dynamic efficiency test. The algorithm tracks the MPP under the irradiation slopes proposed in the standard.

The quality of the MPP tracking is very good and it is similar with all ramps. There is a small lag in all the cases, but it is acceptable because the algorithm has to first detect how the irradiance varies and then set the reference voltage accordingly.

The dynamic efficiency was calculated as follows:

$$\eta_{MPPT} = \frac{P_{PV}}{P_{MPP}} \tag{12}$$

where P_{PV} is the power obtained from the PV panel and P_{MPP} is the theoretical maximum one. The MPP data obtained when the irradiation changes with steps of 5 W/m^2 from 100 to 1000 W/m^2 was used to calculate the MPP power (P_{MPP}) in these points and then using MATLAB$^{®}$ deriving the equation which best fits the points distribution. In order to calculate the dynamic efficiency, 50 points per second were used. The efficiencies under the slopes proposed in Table III are shown in Table IV.

Table IV - Dynamic efficiencies.

Efficiency (%)		Slope [W/m^{2}s]					
		10	14	20	30	50	100
MPPT	P&O	99.5113	99.5084	99.5027	99.4947	99.4832	99.4618
	InCond	99.5106	99.5039	99.5034	99.4949	99.4844	99.4622

The efficiency is over 99.4% in all cases and it is really similar in both algorithms, P&O and InCond. This confirms the claim in [17] that P&O performs similarly to InCond, if it is well optimized.

4.4   Model validation

In order to validate the simplified model described in Section 4.1, its operation was compared to that of a complete model of a grid connected PV system, which includes a three phase inverter. This complete model was developed using PLECS$^{®}$ and Simulink$^{®}$. The switching signals for the three phase inverter are generated by a space vector pulse-width modulation and it was controlled so that its output current had power factor 1. The remaining details of the simulation model of the inverter are beyond the scope of this thesis.

The results obtained with both models are depicted in Figure 27. The irradiation profile changes from 300 to 1000 W/m^2 with a slope of 100 W/m^2/s, then it remains constant for 3 seconds and after that, it decreases again to 300 W/m^2 with the same slope. Such a

steep ramp was used because with the available desktop PCs at the time of this work it was impossible to simulate the detailed PV system with the inverter under other irradiation profiles. Both modified algorithms (P&O and InCond) were tested and the same results were obtained. Other less steep ramps were used as well, but between closer irradiance levels in order to reduce the simulation time. The results from these simulations were similar to these in Figure 27. Hence the simplified model is valid to test the dynamic efficiency of the algorithms with the irradiation profiles proposed in [9].
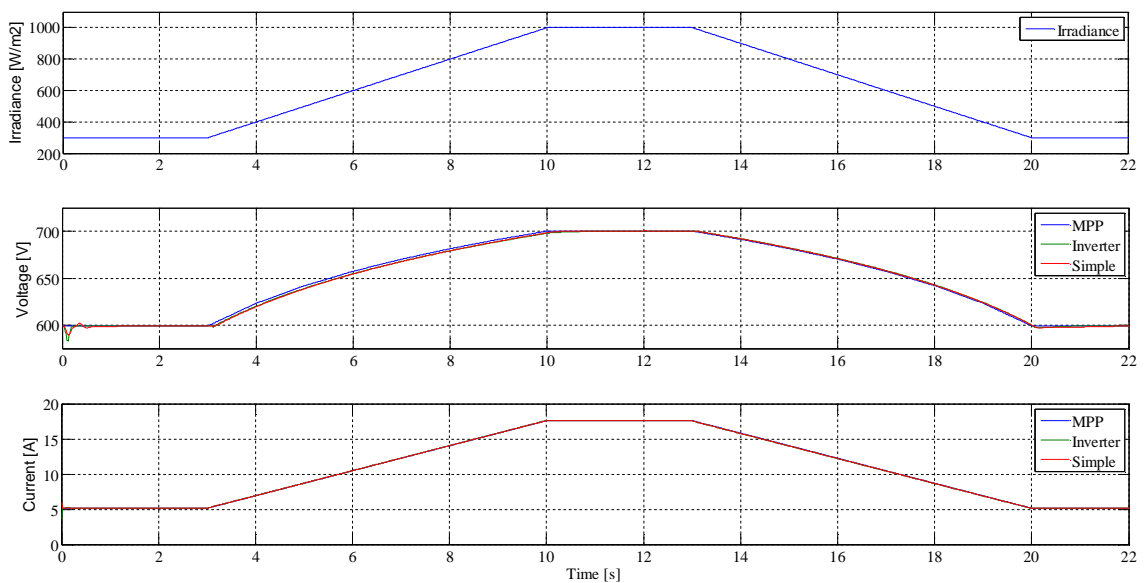
Figure 27 - Comparative between the model with inverter and the simplified one without it. The irradiation slope is 100 W/m²/s. The performance of both models is similar and very good, as the MPP is tracked just with a small lag. The algorithm used is the modified InCond.

4.5 Fuzzy logic controller

In this section, the dynamic MPPT efficiency of a fuzzy logic MPP controller will be evaluated. The parameters of the system are the same used in the previous sections. The only difference is that the MPP Controller block was replaced with the Fuzzy Logic Controller block of Matlab®/Simulink®. The inputs of the inference system are an error and the change in the error as in (7) and (8). The output is the reference voltage, which is later transformed in reference current using the same scheme as in the previous simulations and depicted in Figure 18. Seven triangular membership functions have been used for each variable. They have been chosen not completely symmetric for

better accuracy [8], [25]. The rule base is the one shown in Table I. The sampling frequency of the controller has been set to 500 Hz. More details of the fuzzy inference system (FIS) which is utilized by the fuzzy controller can be found in Appendix B.

The results obtained with the FLC using the FIS previously described are good when the gradients of the slopes are above 10 W/m^2/s, as is depicted in Figure 28 and Figure 29.
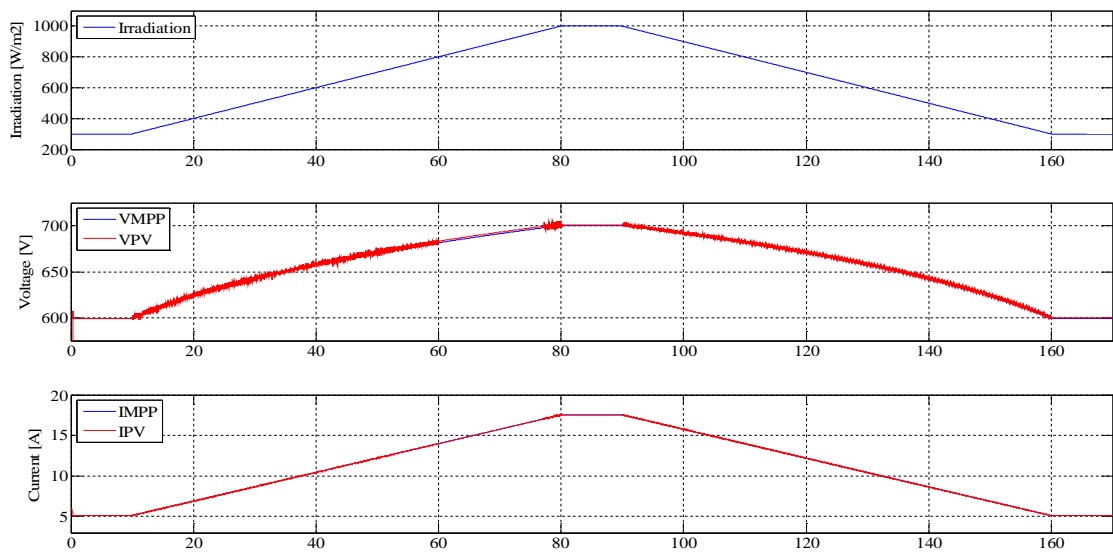

Figure 28 – MPP tracking with a FLC under a slope of 10W/m^2/s.
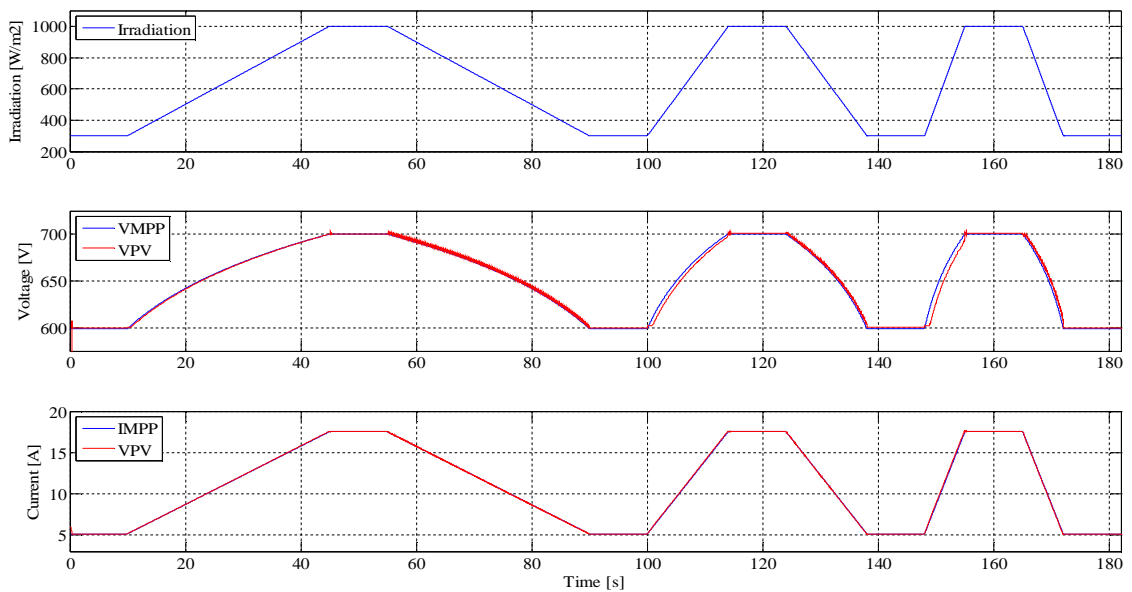
Figure 29 - MPP tracking with a FLC under slopes of 20, 50 and 100 W/m^2/s respectively.

The controller manages to track the MPP in these cases. However, a small ripple exists around the MPP when the gradient is small. With larger gradients there is a small lag. The efficiencies are shown in Table V.

Table V – Dynamic efficiencies with the Fuzzy Logic Control.

Efficiency (%)	Slope [W/m^2/s]			
	10	20	50	100
Fuzzy Logic Control	99.5096	99.5012	99.4754	99.4330

The efficiencies are slightly smaller than with the modified InCond and P&O algorithms, as can be observed comparing Table IV and Table V. Unfortunately, this fuzzy logic control cannot track the MPP under ramps with gradients below 10 W/m^2/s, as shown in Figure 30.
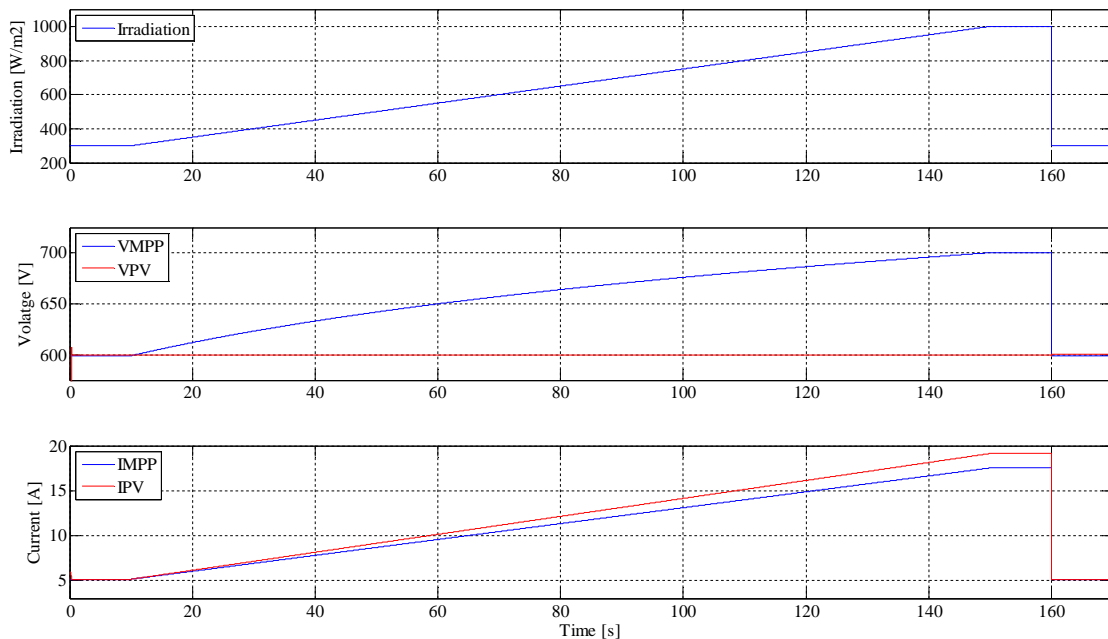
Figure 30 - MPP tracking with a FLC under a slope of 5W/m^2/s.

The problem with small gradients is related to the high sampling frequency used in the fuzzy controller (500 Hz). When the gradients are small, the error and the change in the error are really small and both correspond to the ZERO membership functions, even though these MFs are really narrow in both cases. Consequently, the increment in the

reference voltage is set to zero and the MPP is not correctly tracked. If the sampling frequency is reduced in order to track the MPP under less steep ramps, then the quality in the tracking of the steepest slopes is reduced because the lag becomes bigger. This is due to the fact that the period between the samples is longer so it takes more time to detect the irradiation slope. Therefore the efficiency drops below 99%. Even when the sampling frequency was reduced to 100 Hz, the FLC could not track the MPP when the gradient was below 5 W/m^2/s. In other words, it is difficult to achieve a compromise, some of the slopes proposed in the standard are not tracked well and if the sampling frequency is reduced to track them, then the efficiency with steeper ramps drops dramatically.

4.6   Results comparison

Comparing the performances of the different algorithms considered in this chapter, it can be said that the best results have been obtained with the modified InCond and P&O methods. The dynamic efficiency when using the irradiation slopes in Table III is over 99.4%. Furthermore, the P&O and InCond algorithms track the MPP under all ramps in Table II with even better efficiencies, as seen in Figure 31. The efficiency was 99.6531% and the irradiance varied from 100 to 500 W/m^2 following a slope with a gradient of 1 W/m^2/s. In contrast, using the FLC the efficiencies are good with the slopes from Table III but when the gradients are smaller, then the tracking gets bad because the controller does not detect the change in the irradiation and the reference voltage is kept constant. This leads to a severe drop in the power obtained from the PV array because the MPP is not tracked. Another disadvantage of the FLC is that it is more difficult to tune because all MFs have to be customized for the PV array used in the system. The efficiency of the controller depends greatly on designer's expertise in proposing a suitable FIS for the FLC. The reason is that there are no general rules how to select the MFs or which error should be chosen. In contrast, in the case of the modified hill-climbing techniques, the design steps are well defined. Moreover, the sampling frequency required by the FLC to achieve a similar performance is 20 times greater than in the modified P&O and InCond (500 and 25 Hz respectively) and even in

this case, the FLC does not succeed in tracking the MPP with all the slopes proposed by the standard.
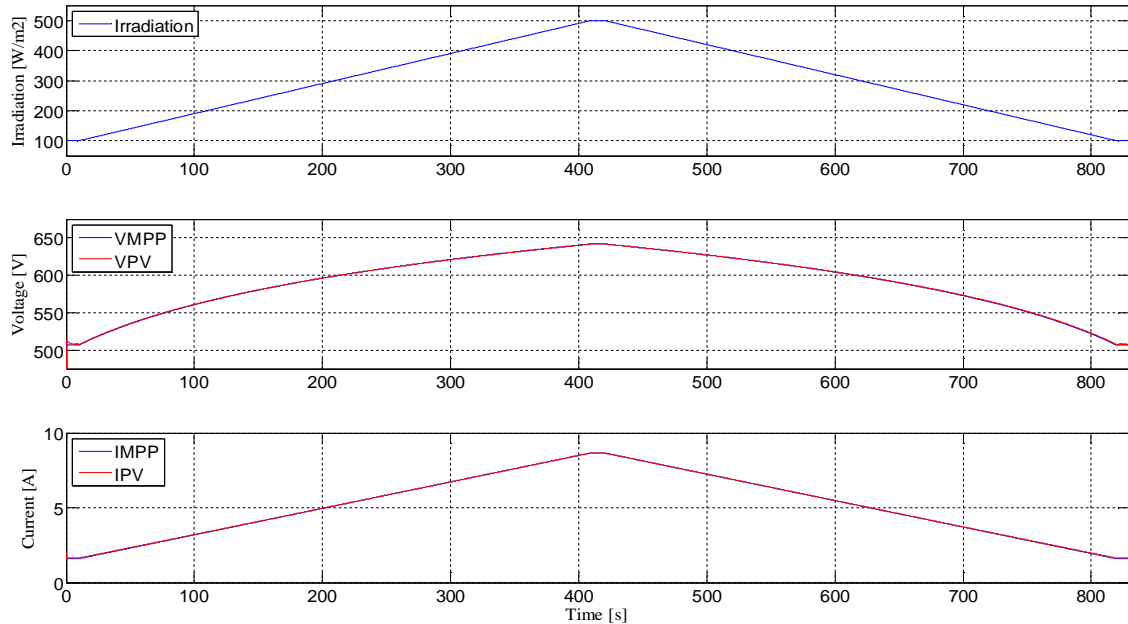

Figure 31 - MPPT tracking with a slope of 1 W/m^2/s from 100 to 500 W/m^2 and the InCond algorithm in the core of the modified scheme. The efficiency is 99.6531%.

In any case, FLC cannot be totally discarded. It is possible that an expert can design a fuzzy controller as efficient as the modified algorithms proposed in these thesis or even better.

Comparing the performance of the modified P&O and InCond algorithms, it can be said that both are very similar. For this reason, the only factor to choose one of them is the simplicity. It can be seen, comparing the flowchart of both algorithms, Figure 12 and Figure 22, that the InCond is a little more complicated, because it requires the division of the power increments by those of the voltage (current), which are later compared to zero; whereas in the P&O method the increments are straight compared to zero, so less operations are required and thus it is a simpler algorithm.

After these considerations, it can be concluded that the best MPPT algorithm is the modified P&O method proposed in this thesis. The only limitation of this algorithm is that it finds the closest local maximum. Multiple maxima can appear in the V-P

characteristic curve when the PV array is partially shaded. In order to overcome this limitation, the P&O algorithm has to be combined with a method that can find the global maximum. The techniques for global MPP searching are not used constantly because their efficiency is not good. Instead, they are used to check periodically if the operating point is near the real MPP. After the check, the controller continues to use the MPPT algorithm that has better efficiency.

5 Conclusions

In this thesis, most of the MPPT algorithms which can find the real MPP were reviewed. For simplicity and effectiveness reasons, P&O, InCond, and FLC were selected for further analysis. Their performance and dynamic MPPT efficiencies were studied according to the European Standard EN 50530. The tests confirmed the problems of P&O and InCond algorithms as reported in the literature.

For testing purposes, a simplified model of the PV system was developed. In this model, the power converter was replaced with a controlled current source. This allowed long enough simulations so that the dynamic MPPT efficiency can be tested.

Modifications to the traditional P&O and InCond algorithms were proposed, which allow the hill-climbing algorithms to track the MPP even under changing irradiation and adapt the increment in the reference voltage to the operating point, as the variation of the MPP voltage is not linear. The dynamic efficiency measured according the standard was above 99.4 %.

The performances of the modified P&O and InCond algorithms and the fuzzy logic were compared and based on the results of the dynamic efficiency tests, it was concluded that the modified hill-climbing algorithms perform better than the FLC. Fuzzy logic cannot be discarded based on these results alone, because the author is not an expert in tuning fuzzy systems. However, no evidences were found of good performance of the FLC under conditions of changing irradiance. In any case, a FLC is more difficult to design and tune.

After, taking into account all the results, it can be concluded that the best algorithm is the modified P&O. Its dynamic MPPT efficiency is similar to that of the modified InCond, but the P&O algorithm is simpler.

The above conclusions are based on simulations and the reported results in the literature. No experimental validation could be done and that should be the next step to confirm the results from the simulations.

References

[1] The European Union climate and energy package, (The "20 – 20 – 20" package), http://ec.europa.eu/clima/policies/eu/package_en.htm [Accessed 28/10/2010].

[2] D. JC. MacKay, "Sustainable Energy - Without the Hot Air", UIT Cambridge, 2009. [Online]. Available: http://www.inference.phy.cam.ac.uk/sustainable/book/tex/cft.pdf, [Accessed 28/10/2010].

[3] "Trends in photovoltaic applications. Survey report of selected IEA countries between 1992 and 2009", International Energy Agency, Report IEA-PVPS Task 1 T1-19:2010, 2010. [Online]. Available: http://www.iea-pvps.org/products/download/Trends-in-Photovoltaic_2010.pdf [Accessed 28/10/2010].

[4] P. A. Lynn, *Electricity from Sunlight: An Introduction to Photovoltaics*, John Wiley & Sons, 2010, p. 238.

[5] "Sunny Family 2010/2011 - The Future of Solar Technology", SMA product catalogue, 2010. [Online]. Available: http://download.sma.de/smaprosa/dateien/2485/SOLARKAT-KUS103936W.pdf [Accessed 14/12/2010].

[6] L. Piegari, R. Rizzo, "Adaptive perturb and observe algorithm for photovoltaic maximum power point tracking," *Renewable Power Generation*, IET, vol. 4, no. 4, pp. 317-328, July 2010.

[7] N. Femia, G. Petrone, G. Spagnuolo, M. Vitelli, "Optimizing sampling rate of P&O MPPT technique," in *Proc. IEEE PESC,* 2004, pp. 1945- 1949.

[8] T. Esram, P.L. Chapman, "Comparison of Photovoltaic Array Maximum Power Point Tracking Techniques," *IEEE Transactions on Energy Conversion*, vol. 22, no. 2, pp. 439-449, June 2007.

[9] *Overall efficiency of grid connected photovoltaic inverters*, European Standard EN 50530, 2010.

[10] T. Markvart, *Solar electricity*, Wiley, 2000, p. 280.

[11] G. M. S. Azevedo, M. C. Cavalcanti, K. C. Oliveira, F. A. S. Neves, Z. D. Lins, "Evaluation of maximum power point tracking methods for grid connected photovoltaic systems," in *Proc. IEEE PESC*, 2008, pp. 1456-1462.

[12] "BP Solar limited warranty certificate", BP Solar, 2010. [Online]. Available: http://www.bp.com/liveassets/bp_internet/solar/bp_solar_usa/STAGING/local_assets/downloads_pdfs/2010_Warranty.pdf [Accessed 14/12/2010].

[13] Norjasmi Bin Abdul Rahman, "Inverter Topologies for Photovoltaic Systems", Master's Thesis, Dept. Electrical Engineering, Aalto University School of Science and Technology, Espoo, Finland, 2010.

[14] Tat Luat Nguyen, Kay-Soon Low, "A Global Maximum Power Point Tracking Scheme Employing DIRECT Search Algorithm for Photovoltaic Systems," *IEEE Transactions on Industrial Electronics*, vol. 57, no. 10, pp. 3456-3467, Oct. 2010.

[15] D. Sera, T. Kerekes, R. Teodorescu, F. Blaabjerg, "Improved MPPT Algorithms for Rapidly Changing Environmental Conditions," in *Proc. 12th International Conference on Power Electronics and Motion Control*, 2006, pp. 1614-1619.

[16] D. Sera, T. Kerekes, R. Teodorescu, F. Blaabjerg, "Improved MPPT method for rapidly changing environmental conditions," in *Proc. IEEE International Symposium on Industrial Electronics*, 2006, vol. 2, pp. 1420-1425.

[17] N. Femia, G. Petrone, G. Spagnuolo, M. Vitelli, "Optimization of perturb and observe maximum power point tracking method," *IEEE Transactions on Power Electronics*, vol. 20, no. 4, pp. 963-973, July 2005.

[18] K.H. Hussein, I. Muta, T. Hoshino, M. Osakada, "Maximum photovoltaic power tracking: an algorithm for rapidly changing atmospheric conditions," *IEE Proceedings on Generation, Transmission and Distribution*, vol. 142, no. 1, pp. 59-64, Jan 1995.

[19] C. Zhang, D. Zhao, J. Wang, G. Chen, "A modified MPPT method with variable perturbation step for photovoltaic system," in *Power Electronics and Motion Control Conference*, 2009, pp. 2096-2099.

[20] W. Xiao, W. G. Dunford, "A modified adaptive hill climbing MPPT method for photovoltaic power systems," in *Proc. IEEE PESC*, 2004, pp. 1957-1963.

[21] S. Jain, V. Agarwal, "Comparison of the performance of maximum power point tracking schemes applied to single-stage grid-connected photovoltaic systems," *Electric Power Applications*, IET, vol. 1, no. 5, pp. 753-762, Sept. 2007.

[22] P. Midya, P. T. Krein, R. J. Turnbull, R. Reppa, and J. Kimball, "Dynamic maximum power point tracker for photovoltaic applications," in *Proc. 27th Annual IEEE Power Electronics Specialists Conference*, 1996, pp. 1710-1716.

[23] N. Patcharaprakiti, S. Premrudeepreechacharn, "Maximum power point tracking using adaptive fuzzy logic control for grid-connected photovoltaic system," in *Proc. IEEE Power Engineering Society Winter Meeting*, 2002, pp. 372-377.

[24] Chao Zhang, Dean Zhao, "MPPT with asymmetric fuzzy control for photovoltaic system," in *Proc. 4th IEEE Conference on Industrial Electronics and Applications*, 2009, pp. 2180-2183.

[25] J. Li, H. Wang, "Maximum power point tracking of photovoltaic generation based on the fuzzy control method," in *Proc. International Conference on Sustainable Power Generation and Supply*, 2009, pp. 1-6.

[26] T. Noguchi, S. Togashi, R. Nakamoto, "Short-current pulse-based maximum-power-point tracking method for multiple photovoltaic-and-converter module system," *IEEE Transactions on Industrial Electronics*, vol. 49, no. 1, pp. 217-223, Feb 2002.

[27] S. Yuvarajan, S. Xu, "Photo-voltaic power converter with a simple maximum-power-point-tracker," in *Proc. International Symposium on Circuits and Systems*, 2003, vol. 3, pp. 399-402.

[28] B. Bekker, H. J. Beukes, "Finding an optimal PV panel maximum power point tracking method," in *Proc. 7th AFRICON Conference in Africa*, 2004, vol. 2, pp. 1125-1129.

[29] M. Bodur, M. Ermis, "Maximum power point tracking for low power photovoltaic solar panels," in *Proc. 7th Mediterranean Electrotechnical Conference*, 1994, vol. 2, pp. 758-761.

[30] E. V. Solodovnik, S. Liu, and R. A. Dougal, "Power Controller Design for Maximum Power Tracking in Solar Installations," *IEEE Transactions in Power Electronics*, vol. 19, pp. 1295-1304, Sept. 2004.

[31] J. A. Gow, C. D. Manning, "Development of a photovoltaic array model for use in power-electronics simulation studies," *IEE Proceedings on Electric Power Applications*, vol. 146, no. 2, pp. 193-200, Mar 1999.

[32] H. L. Tsai, C. S. Tu, Y. J. Su, "Development of Generalized Photovoltaic Model Using MATLAB/SIMULINK," in *Proc. World Congress on Engineering and Computer Science*, 2008, pp. 846-854.

[33] I. H. Altas, A. M. Sharaf, "A Photovoltaic Array Simulation Model for Matlab-Simulink GUI Environment," in *Proc. International Conference on Clean Electrical Power*, 2007, pp. 341-345.

[34] D. Sera, R. Teodorescu, P. Rodriguez, "PV panel model based on datasheet values," in *Proc. IEEE International Symposium on Industrial Electronics*, 2007, pp. 2392-2396.

[35] E. Ritchie, K. M. Leban, "Selecting the Accurate Solar Panel Simulation Model," in *Proc. NORPIE*, 2008, pp. 1-7.

[36] F. Khan, S.N. Singh, M. Husain, "Determination of diode parameters of a silicon solar cell from variation of slopes of the I-V curve at open circuit and short circuit conditions with the intensity of illumination", *Semiconductor Science and Technology*, vol. 25, no. 1, pp. 015002, Jan. 2010.

[37] H. Häberlin, "New test procedure for Measuring Dynamic MPP Tracking Efficiency at Grid connected PV inverters," in *24th European Photovoltaic Solar Energy Conference*, Hamburg, 2009, p. 7.

[38] M. Valentini, A. Raducu, D. Sera, R. Teodorescu, "PV inverter test setup for European efficiency, static and dynamic MPPT efficiency evaluation," in *Proc. 11th International Conference on Optimization of Electrical and Electronic Equipment*, 2008, pp. 433-438.

Appendix A – Results of the Dynamic Efficiency Tests

The results from the dynamic efficiency tests of the hill-climbing algorithms presented in Chapter 4 are shown in this appendix.

Original incremental conductance algorithm

Figure 32 depicts the MPP tracking of this algorithm under irradiation slopes with gradients of 20 and 100 W/m^2/s. Obviously, under such irradiation slopes, this method is unable to track the MPP.
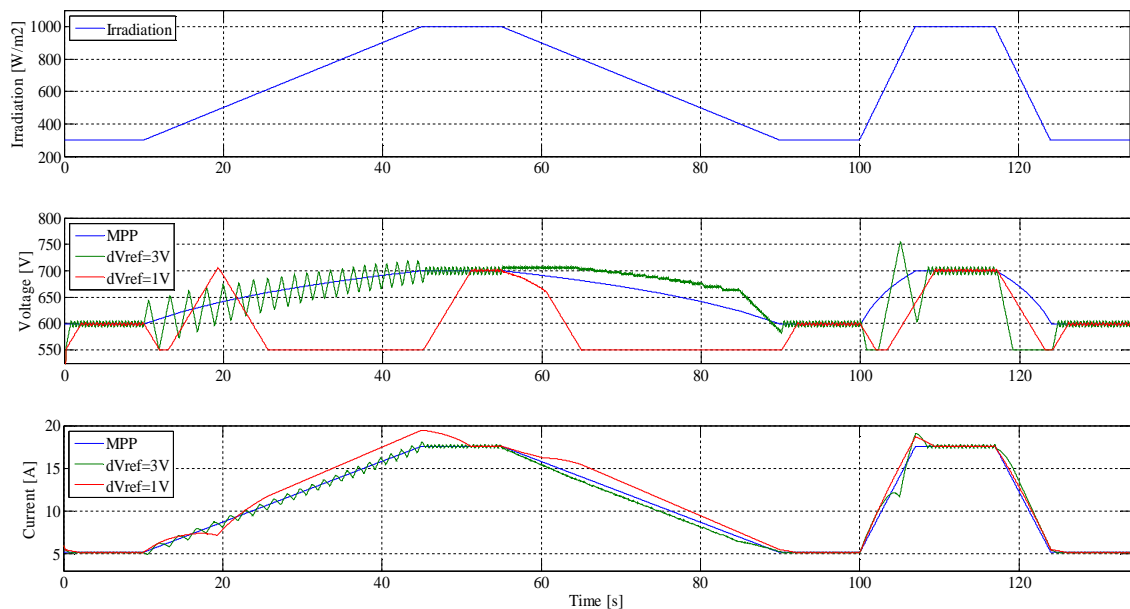
Figure 32 - Performance of the InCond original algorithm under slopes of 20 and 100 W/m^2/s.

Figure 33 shows the performance of the algorithm under irradiation step changes. This time the algorithm tracks the MPP because the change is instantaneous. The convergence speed and the amplitude of the oscillations are directly related to the size of the increment in the reference voltage. A compromise must be found, because it is impossible to reduce the oscillation and at the same time have a high convergence speed.
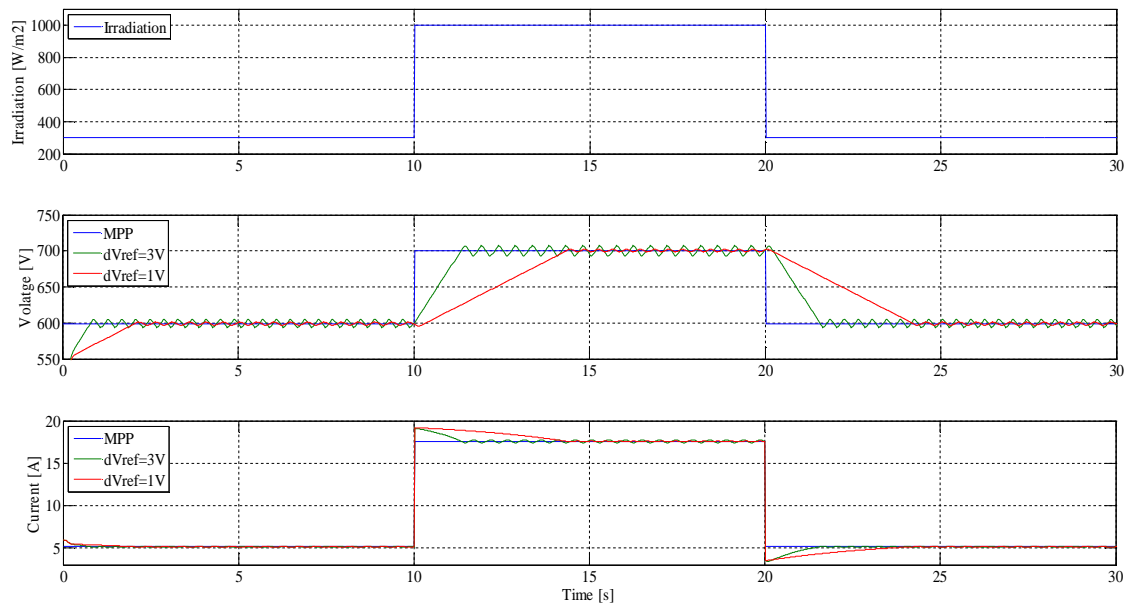
Figure 33 - Performance of the InCond original algorithm under step changes from 300 to 1000 W/m².

Modified algorithms under conditions of changing irradiance

The modified algorithms (P&O and InCond) have been tested under all the slopes proposed in the standard. Because the performance in all case is very similar it is not necessary to show the results from all tests. Table VI lists the results from the dynamic MPPT efficiency tests that are included in the thesis together with their locations.

Table VI - Tests included in the thesis.

Slope (W/m²/s)	Rise time (s)	Dwell time (s)	Simulation time (s)	Location in the thesis
0.50	800.00	10.00	1630.00	Appendix A
1.00	400.00	10.00	830.00	Appendix A
5.00	140.00	10.00	310.00	Appendix A
10.00	70.00	10.00	170.00	Appendix A
14.00	50.00	10.00	130.00	Appendix A
20.00	35.00	10.00	100.00	Section 4.3
30.00	23.33	10.00	76.67	Appendix A
50.00	14.00	10.00	58.00	Section 4.3
100.00	7.00	10.00	44.00	Section 4.3

All results consist of three plots: the first one depicts the irradiation, the second one shows the voltages and the third one the currents. There are two voltages and two currents in the plots, the theoretical MPP values in blue and the actual values of the PV array in red.

Modified perturb and observe algorithm under irradiation slopes

The following figures show the performance of the modified P&O technique under the irradiation slopes detailed in Table VI. At the end of this section a table with all the efficiencies of these tests can be found.
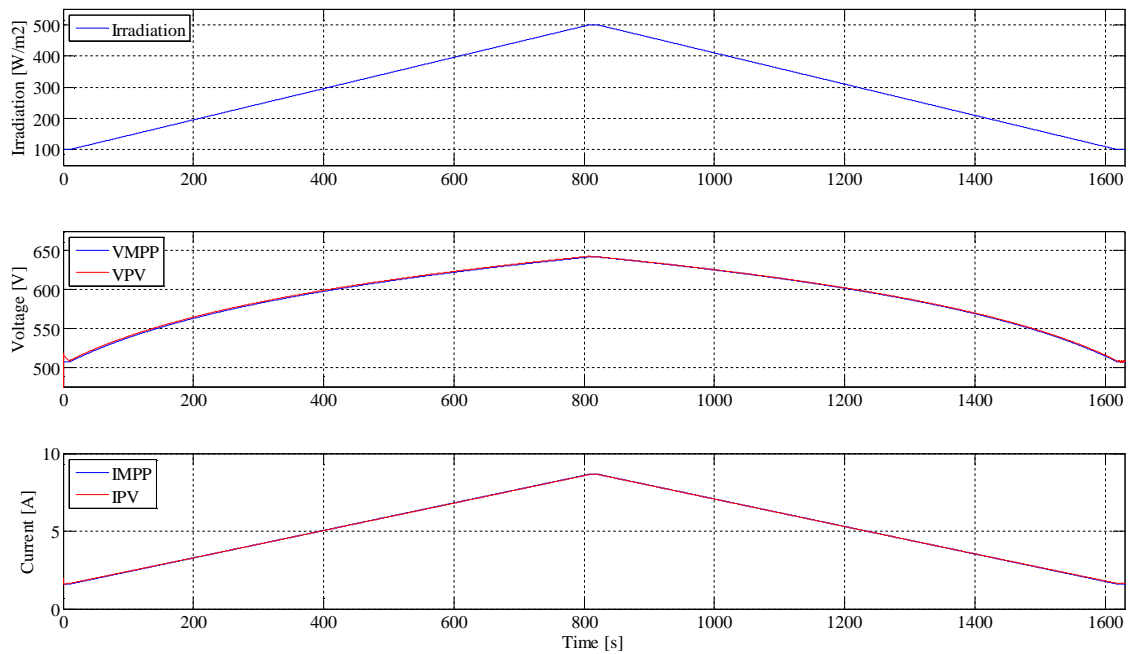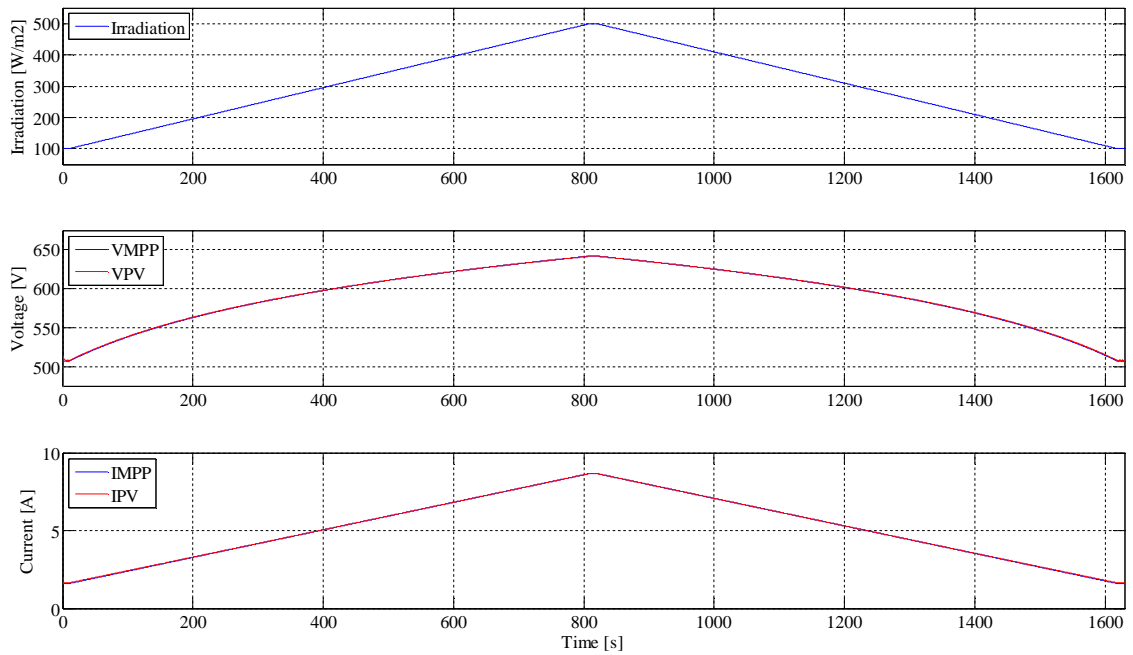

Figure 34 - Performance of the modified P&O algorithm under a slope of 0.5 W/m^2/s.
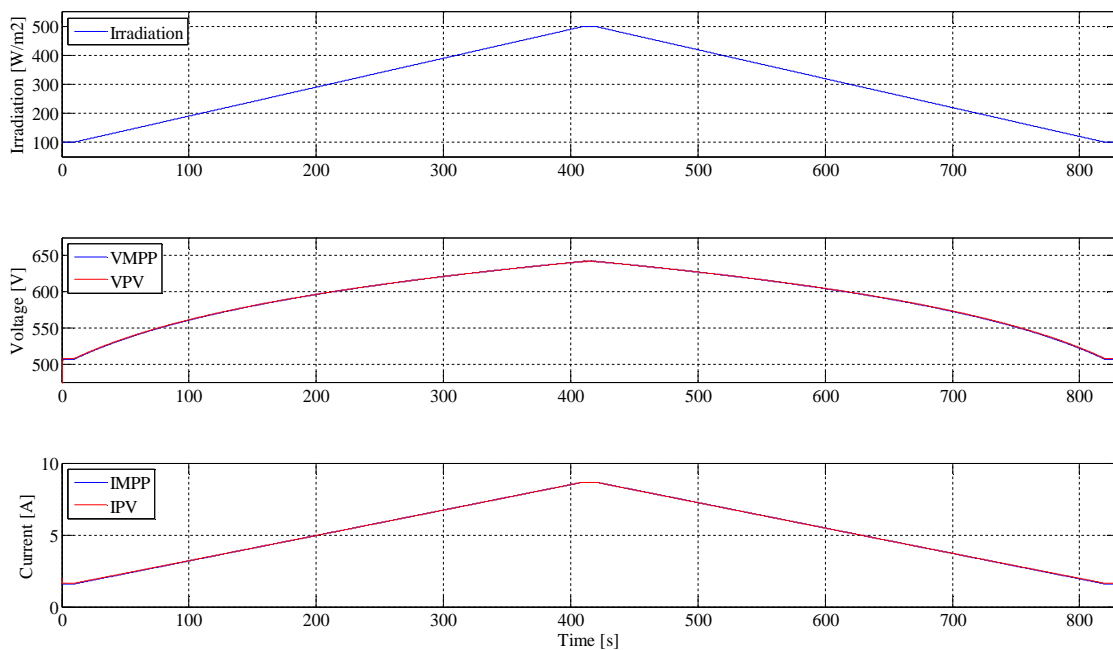
Figure 35 - Performance of the modified P&O algorithm under a slope of 1 W/m^2/s.
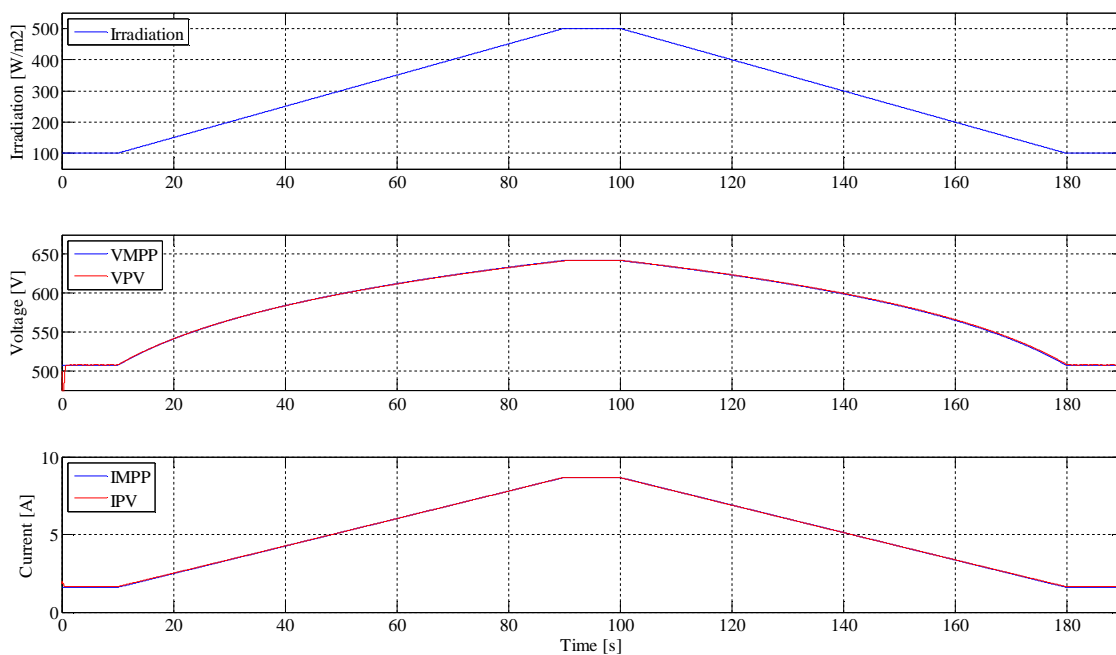
Figure 36 - Performance of the modified P&O algorithm under a slope of 5 W/m^2/s.
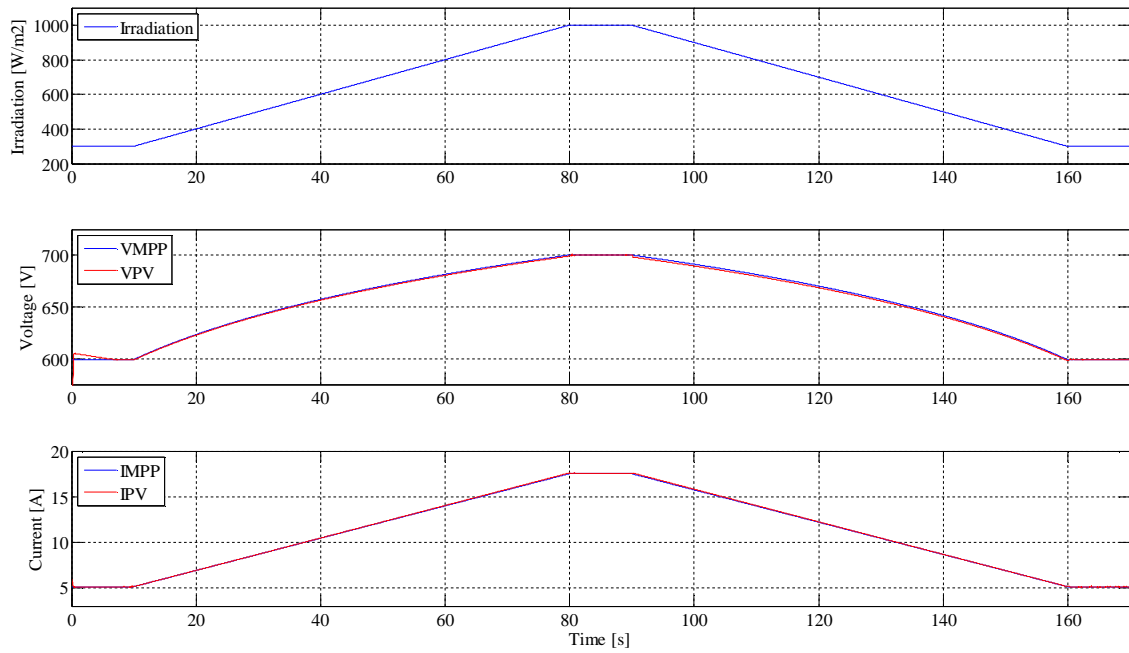
Figure 37 - Performance of the modified P&O algorithm under a slope of 10 W/m²/s.
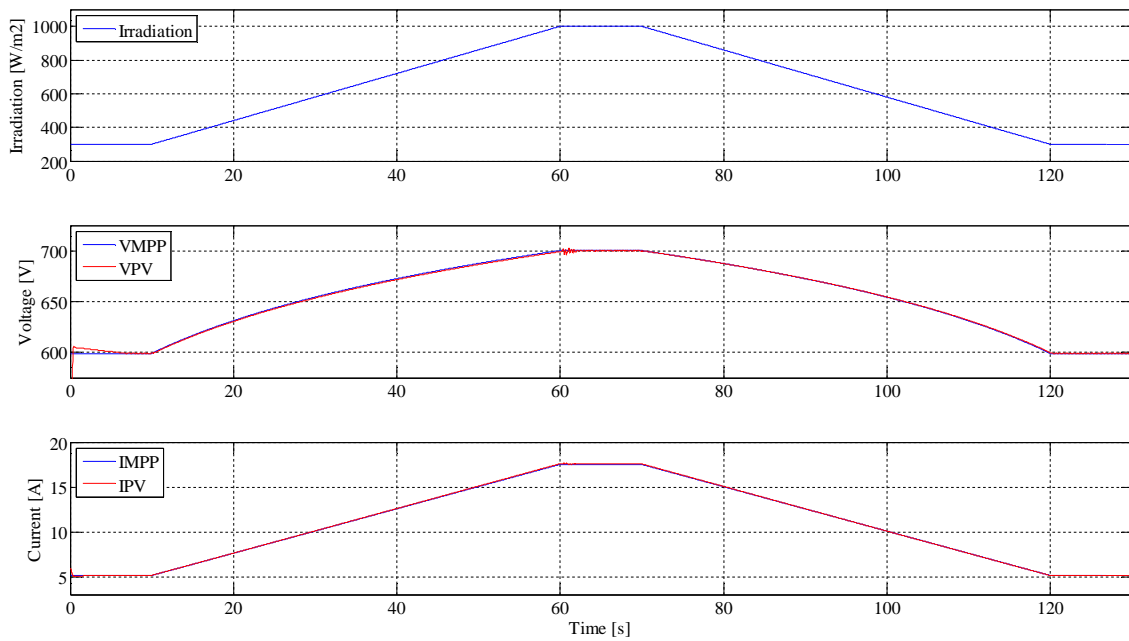
Figure 38 - Performance of the modified P&O algorithm under a slope of 14 W/m²/s.
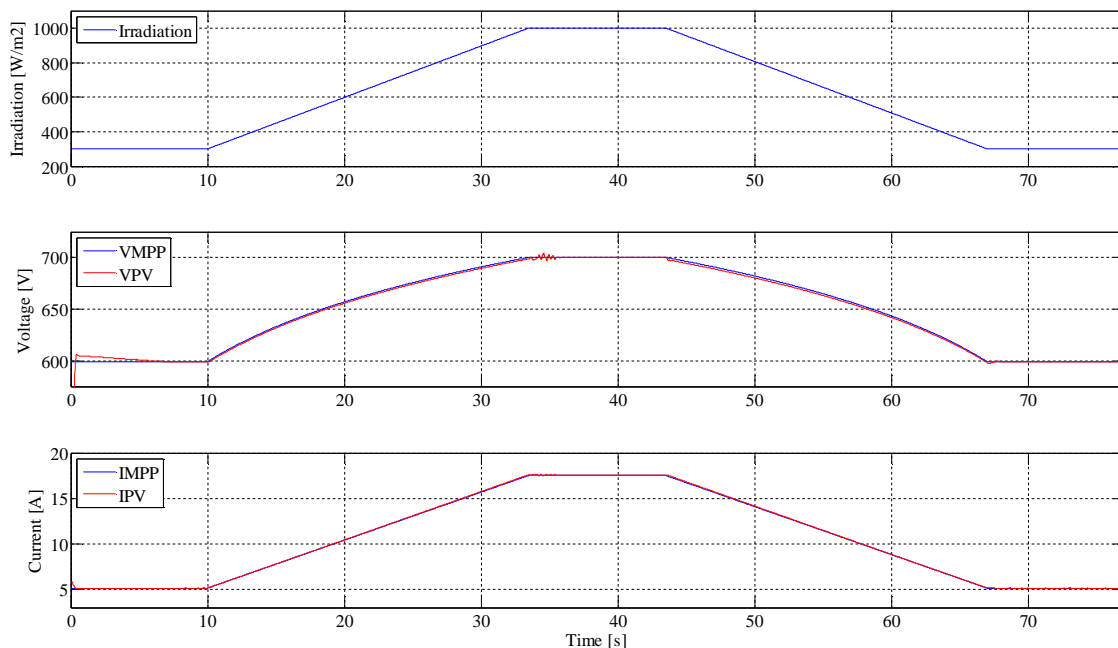
Figure 39 - Performance of the modified P&O algorithm under a slope of 30 W/m^2/s.

The efficiencies of the previous examples are shown in the following Table VII.

Table VII - Dynamic efficiencies of the modified P&O algorithm.

Slope (W/m^2/s)	Efficiency (%)
0.50	99.6532
1.00	99.6585
5.00	99.6864
10.00	99.5113
14.00	99.5084
20.00	99.5027
30.00	99.4947
50.00	99.4832
100.00	99.4618

Modified incremental conductance algorithm under irradiation slopes

The following figures show the performance of the modified InCond technique under the irradiation slopes listed in Table VI. At the end of this section a table with all the efficiencies of these tests can be found.

Figure 40 - Performance of the modified InCond algorithm under a slope of 0.5 W/m^2/s.

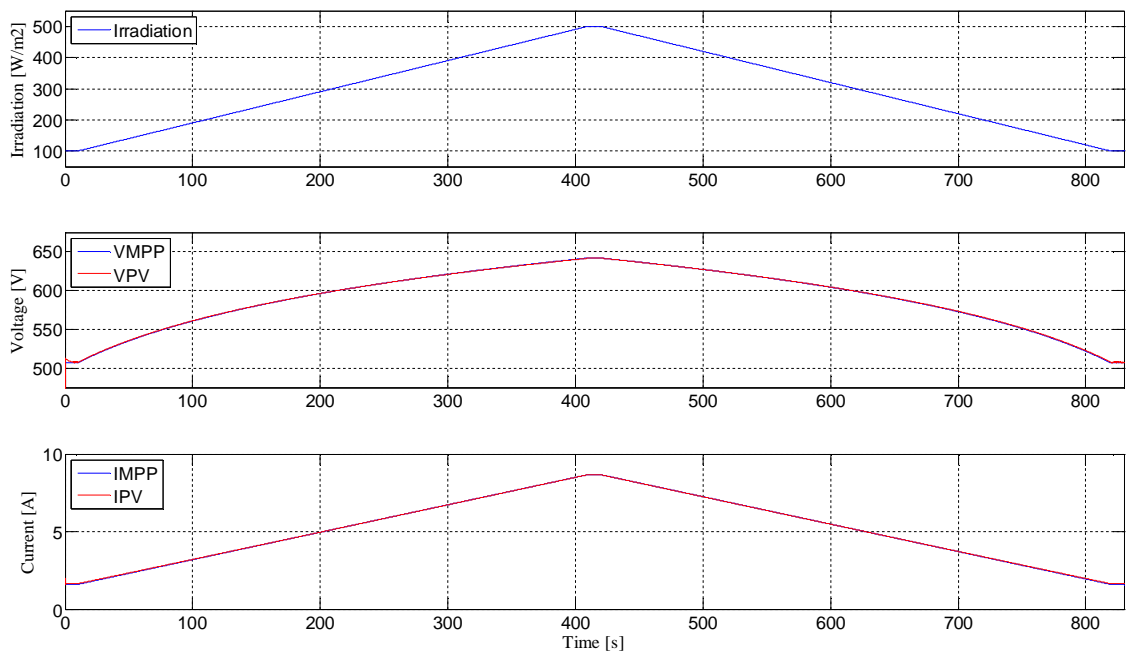**Figure 41 - Performance of the modified InCond algorithm under a slope of 1 W/m^2/s.**

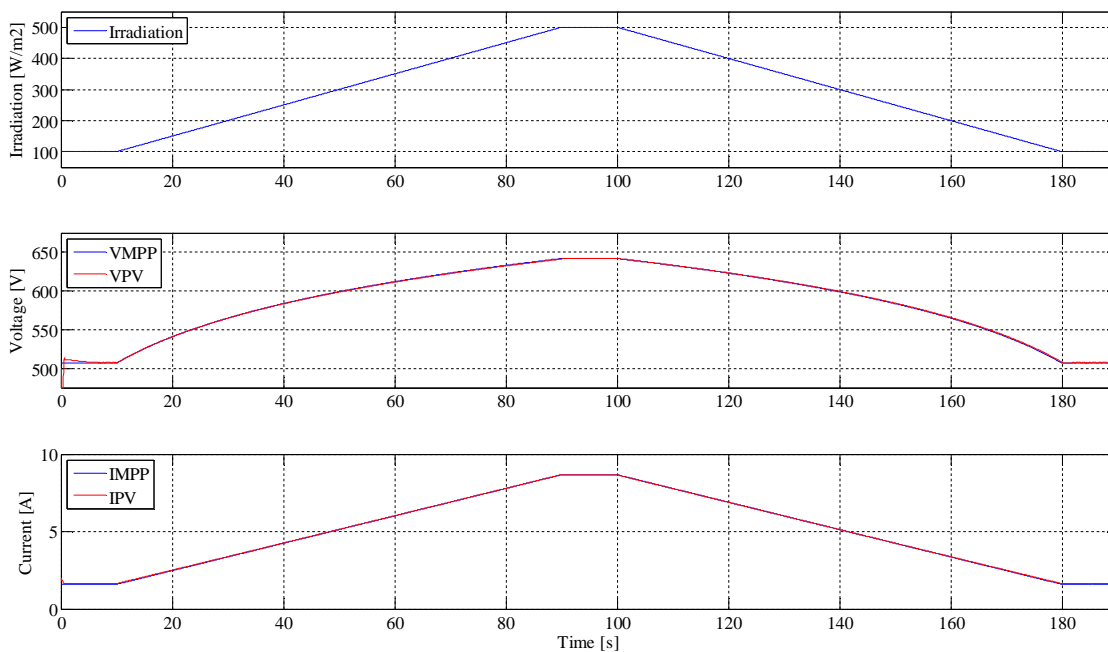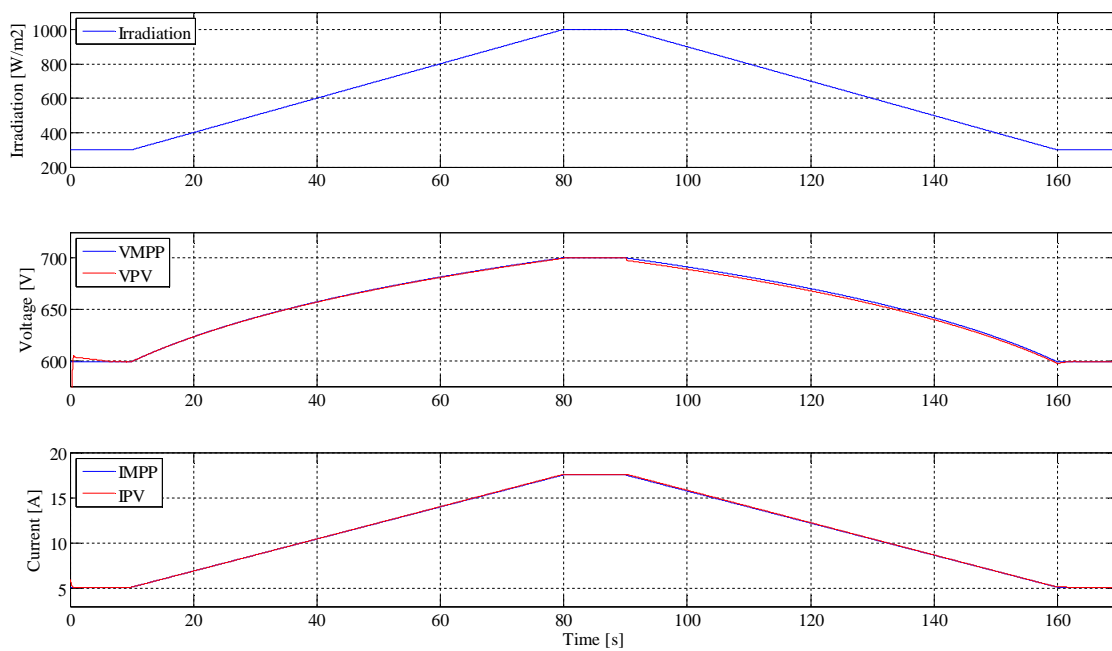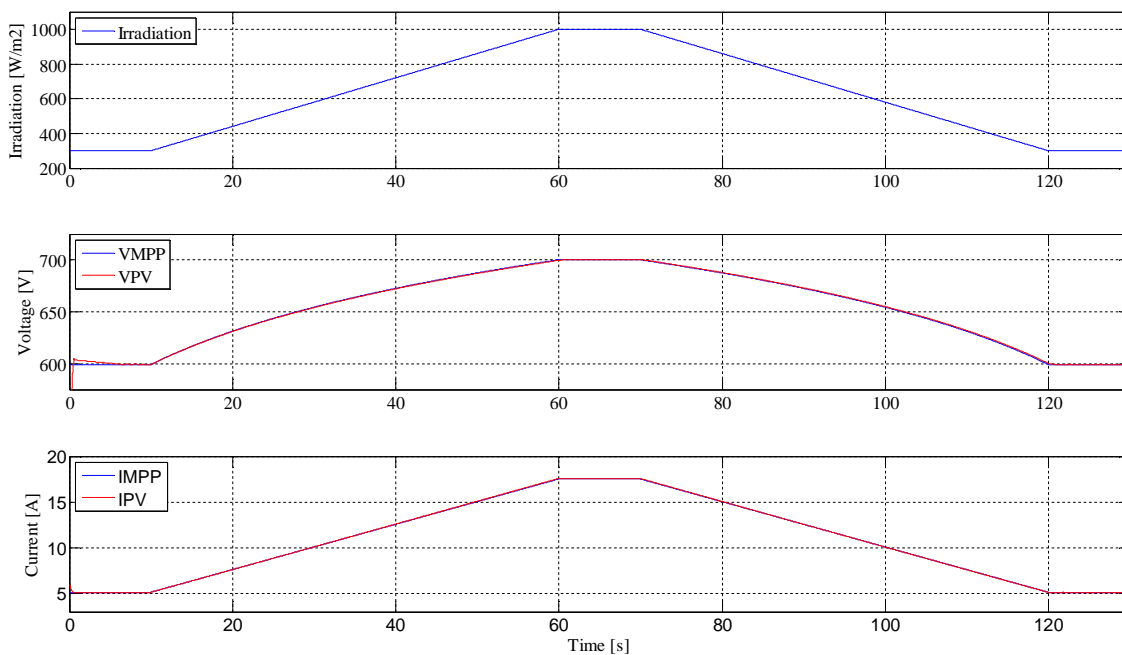**Figure 42 - Performance of the modified InCond algorithm under a slope of 5 W/m^2/s.**

Figure 43 - Performance of the modified InCond algorithm under a slope of 10 W/m^2/s.

Figure 44 - Performance of the modified InCond algorithm under a slope of 14 W/m^2/s.

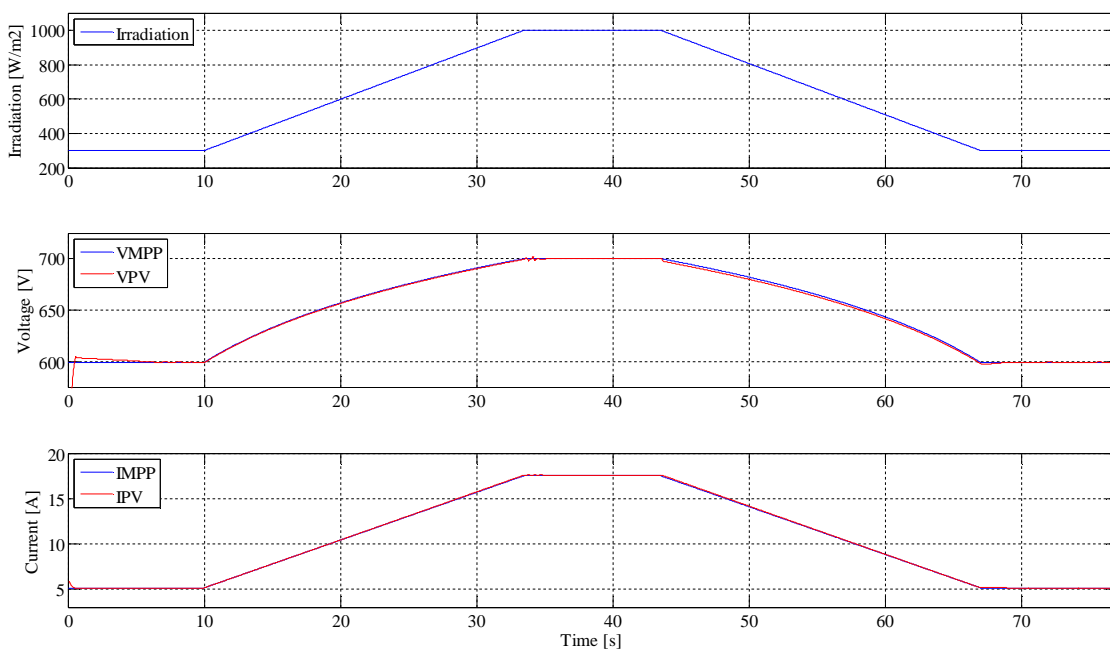**Figure 45 - Performance of the modified InCond algorithm under a slope of 30 W/m^2/s.**

The efficiencies of the previous examples are shown in the following Table VIII.

Table VIII - Dynamic efficiencies of the modified InCond algorithm.

Slope (W/m^2/s)	Efficiency (%)
0.50	99.6503
1.00	99.6531
5.00	99.6588
10.00	99.5106
14.00	99.5039
20.00	99.5034
30.00	99.4949
50.00	99.4844
100.00	99.4622

Appendix B – Fuzzy Inference System for the Fuzzy Logic Controller

Characteristics of the fuzzy logic controller

The inputs of the fuzzy logic controller are an error and the change of the error. They are defined as in equations (7) and (8). For reader's convenience, they are shown again in this section. The output is an increment in the reference voltage.

$$E = \frac{P(k) - P(k-1)}{V(k) - V(k-1)} \tag{7}$$

$$\Delta E = E(k) - E(k-1) \tag{8}$$

Each of the previous variables has seven fuzzy levels represented by the membership functions. To build the MFs related to the input variables, it was taken into account the characteristics of the V-P curves with different irradiance levels, shown in Figure 14, and how they vary.
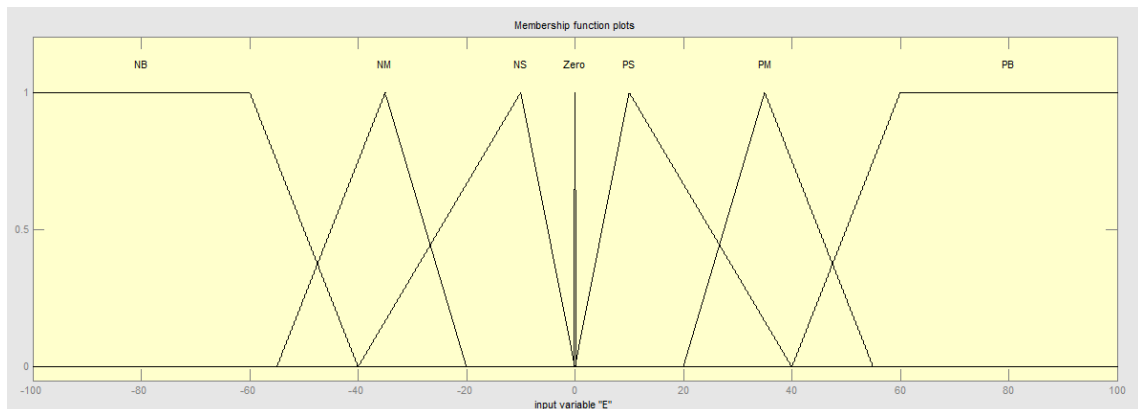

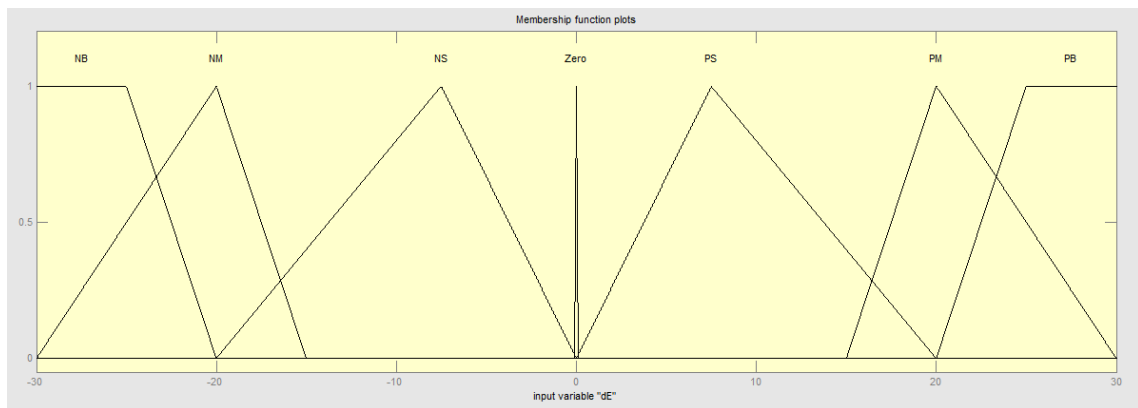**Figure 46 – Membership functions of the input variable *E* (Error).**

Figure 47 - Membership functions of the input variable ΔE (increment in the error).

To design the MFs of the output variable, it was taken into account how large the increment in the reference voltage should be depending on how close to the MPP is the operating point.
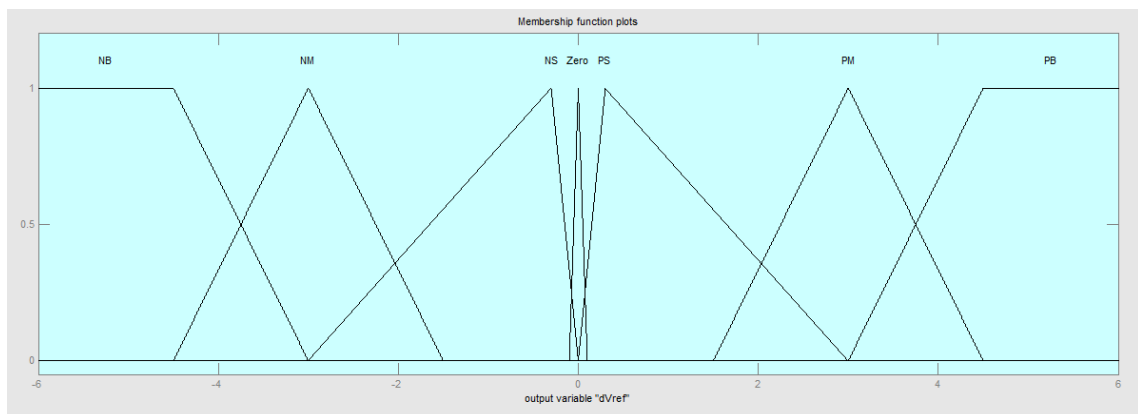

Figure 48 - Membership functions of the output variable ΔV_{ref} (increment in the reference voltage).

After the theoretical design, all the MFs were adjusted by a trial an error process to obtain the desired performance.

The rules are the same shown in Table I, which is again shown here for reader's convenience.

Table IX - Rule base used in the fuzzy controller.

E\dE	NB	NM	NS	ZE	PS	PM	PB
NB	NB	NB	NB	NB	NM	NS	ZE
NM	NB	NB	NB	NM	NS	ZE	PS
NS	NB	NB	NM	NS	ZE	PS	PM
ZE	NB	NM	NS	ZE	PS	PM	PB
PS	NM	NS	ZE	PS	PM	PB	PB
PM	NS	ZE	PS	PM	PB	PB	PB
PB	ZE	PS	PM	PB	PB	PB	PB